Accepted Manuscript

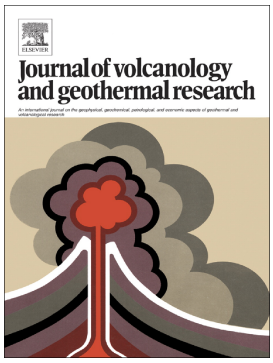


# Eruption of magmatic foams on the moon: Formation in the waning stages of dike emplacement events as an explanation of "irregular mare patches"

Lionel Wilson, James W. Head

PII: S0377-0273(16)30370-5
DOI: doi: 10.1016/j.jvolgeores.2017.02.009
Reference: VOLGEO 6012

To appear in: *Journal of Volcanology and Geothermal Research*

Received date: 23 September 2016
Revised date: 31 January 2017
Accepted date: 7 February 2017

Please cite this article as: Lionel Wilson, James W. Head , Eruption of magmatic foams on the moon: Formation in the waning stages of dike emplacement events as an explanation of "irregular mare patches". The address for the corresponding author was captured as affiliation for all authors. Please check if appropriate. Volgeo(2017), doi: 10.1016/j.jvolgeores.2017.02.009

This is a PDF file of an unedited manuscript that has been accepted for publication. As a service to our customers we are providing this early version of the manuscript. The manuscript will undergo copyediting, typesetting, and review of the resulting proof before it is published in its final form. Please note that during the production process errors may be discovered which could affect the content, and all legal disclaimers that apply to the journal pertain.

ACCEPTED MANUSCRIPT



# Eruption of Magmatic Foams on the Moon: Formation in the Waning Stages of Dike Emplacement Events as an Explanation of "Irregular Mare Patches"

Lionel Wilson[1,2] and James W. Head[2]

[1]Lancaster Environment Centre, Lancaster University, Lancaster LA1 4YQ, UK;
l.wilson@lancaster.ac.uk

[2]Department of Earth, Environmental and Planetary Sciences,
Brown University, Providence, RI 02912, USA

Submitted to *Journal of Volcanology and Geothermal Research*
September 23, 2016

Key words: Lunar/Moon, mare volcanism, irregular mare patches, strombolian, magmatic foam, lava lake, dike emplacement.

ACCEPTED MANUSCRIPT

ACCEPTED MANUSCRIPT



**Abstract**

Volcanic eruptions on the Moon take place in conditions of low gravity and negligible atmospheric pressure, very different from those on Earth. These differences lead to characteristic lunar versions of Hawaiian and strombolian explosive activity, and to the production of unusual eruption products neither predicted nor observed on Earth in the terminal stages of eruptions. These include the unusual mounds and rough (hummocky, blocky) floors of some small-shield summit pit crater floors, elongate depressions and mare flows (similar to those named "irregular mare patches", IMPs, by Braden et al., 2014). We examine the ascent and eruption of magma in the waning stages of the eruptive process in small-shield summit pit crater floors and show that many IMP characteristics can be plausibly explained by basaltic magma behavior as the rise rate of the ascending magma slows to zero, volatiles exsolve in the dike and lava lake to form a very vesicular foam, and the dike begins to close. Stresses in the very vesicular and porous lava lake crust produce fractures through which the foam extrudes at a rate determined by its non-Newtonian rheology. Waning-stage extrusion of viscous magmatic foams to the surface produces convex mounds whose physical properties inhibit typical impact crater formation and regolith development, creating an artificially young crater retention age. This mechanism for the production and extrusion of very vesicular magmatic foams is also applicable to waning-stage dike closure associated with pit craters atop dikes, and fissure eruptions in the lunar maria, providing an explanation for many irregular mare patches. This mechanism implies that IMPs and associated mare structures (small shields, pit craters and fissure flows) formed synchronously billions of years ago, in contrast to very young ages (less than ~100 million years) proposed for IMPs by some workers.

ACCEPTED MANUSCRIPT

ACCEPTED MANUSCRIPT


## 1. Introduction

Obvious differences between the conditions under which volcanic eruptions take place on the Earth and Moon are (i) the lower acceleration due to gravity on the Moon, (ii) the absence of any significant atmospheric pressure on the Moon, (iii) the propensity for lunar eruptions to be fed by dikes from the upper mantle that extend through the crust, delivering mafic magmas, and (iv) the likelihood that all lunar eruptions begin with an explosive phase (Wilson and Head, 1981, 2016; Head and Wilson, 1992, 2016). An important similarity between lunar and terrestrial mafic eruptions is the significance of the presence of magmatic water exsolved in the final stages of approach of magma to the surface. In the lunar case, however, water release in lunar magmas can produce an extremely vesicular foam that is stable on the time scale of an eruption.

In this analysis, we begin with an examination of the likely sequence of events in eruptions associated with small shield volcanoes on the Moon (Head and Gifford, 1980) and use as an example the Ina shield volcano and summit pit crater (Strain and El Baz, 1980; Garry et al., 2012) (Fig. 1a); we then apply our results to several related types of features (linear pit craters and potential examples of late stage fissure eruptions) (Fig. 1b, c). Following recent work on the generation, ascent and eruption of magma on the Moon (Wilson and Head, 2016; Head and Wilson, 2016) we show that features inside summit pit craters, linear pit craters, and other similar structures (mounds and surrounding rough hummocky and blocky floor terrain; defined and described as "irregular mare patches", or IMPs, by Braden et al., 2014) can be understood in terms of lunar volcanic eruptions in which the late stage of an eruptive episode involves the formation and extrusion of very vesicular lava (foam) at a very low volume flux. Overall the eruption has three stages: (i) a nearly steady, high volume flux hawaiian fire fountain explosive stage, (ii) an intermittent, lower volume flux strombolian explosive phase, with these first stages being controlled almost entirely by CO gas release, and (iii) a final very low volume flux effusive stage in which a water vapor-dominated foam is extruded. We outline these steps, discuss the final predicted landforms, and assess the relationship with observed features at small lunar shields. We then apply the same concepts to other candidate late-stage eruptive deposits.

ACCEPTED MANUSCRIPT


**2. Physics of lunar eruptions**

The absence of any atmosphere on the Moon means that, on approaching the surface, all magmas will attempt to release all of the volatile species that they contain in solution or that they can generate by chemical reactions at low pressures. A common component of mafic melts in the lunar mantle is graphite, and reactions between graphite and various metal oxides produce CO gas (Sato, 1976. 1979; Fogel and Rutherford, 1995; Nicholis and Rutherford, 2006, 2009; Wetzel et al., 2015; Rutherford et al., 2015) at a pressure of ~40 MPa (Nicholis and Rutherford, 2009) which occurs at ~10 km depth (Fig. 2a). This gas production ensures that essentially all lunar eruptions begin with an explosive phase (Fig. 2b). The initial stage of the eruption is fed by a dike that is likely to extend completely through the lunar crust into the upper mantle (Wilson and Head, 2016) and the great width of this dike ensures a relatively high magma discharge rate (Fig. 2c).

As the initially high excess pressure in the dike is lost and the dike begins to close due to the elastic response of the crust, the discharge rate must decrease and eventually become very small (Figs. 2d-2f). The discharge rate, i.e. the volume flux, is the product of the cross sectional area of the dike and the magma rise speed within it. As the dike closes, wall friction becomes ever more important and the magma rise speed decreases (Wilson and Head, 1981). Initially, the magma rise speed is so great that gas bubbles nucleating in the magma will have buoyancy-driven rise speeds through the magmatic liquid that are orders of magnitude smaller than the rise speed of the magma itself through the dike (Figs. 2a-2c). This means that an essentially uniform distribution of gas bubbles exists in the magma as it reaches the surface, and the expansion of these bubbles into the lunar vacuum causes the magma to fragment into sub-mm-sized droplets that emerge in a nearly steady hawaiian-style eruption (Fig. 2b). However, as the magma speed decreases, the difference between the magma speed and the bubble speeds becomes less, and the greater transit time allows large bubbles to overtake small ones and coalesce with them (Fig. 2d). At a sufficiently small magma rise speed the process reaches a run-away state, with occasional very large gas bodies - giant bubbles or elongate gas slugs - emerging though a lava lake in the vent and bursting as they expand into the vacuum - this is strombolian activity (Figs. 2d, 3). As the magma rise speed at depth approaches zero (Fig. 2d), the last magma to pass through the 40 MPa pressure level delivers the last strombolian explosion at the surface and the remaining closure of the dike squeezes out magma in which the only gas production is the release of water

ACCEPTED MANUSCRIPT


vapor (Figs. 2e-2f). At the several hundred ppm water contents typical of many lunar magmas (Saal et al., 2008; Hauri et al., 2011, 2015) the gas bubble sizes are so small that surface tension forces allow them to remain stable against the internal gas pressures and so to form a foam that can have a vesicularity up to ~95%. This is the last material to be extruded and we show that it can extend for up to several hundred meters below the surface (Fig. 2f). Using the geometry and dimensions of a specific shield and summit pit crater as examples, we now examine the three major phases (hawaiian, strombolian, foam formation/extrusion) of the eruption in detail.

**3. Hawaiian explosive phase**

In terrestrial hawaiian eruptions the expansion of the released volatiles stops when atmospheric pressure is reached. In contrast, eruptions into a vacuum allow gases to expand indefinitely in all directions and so the lunar equivalent of a relatively steady hawaiian-style eruption is an umbrella-shaped structure like the eruption plumes seen on Io (Wilson and Head, 2016) (Fig. 2b). We assume that lunar explosive activity was dominated by two gas species, CO produced by carbon-metal oxide smelting reactions generating up to 2000 ppm by mass gas (Sato, 1976, 1979; Fogel and Rutherford, 1995; Nicholis and Rutherford, 2006, 2009; Wetzel et al., 2015) and water present in amounts up to ~1000 ppm at depth (Saal et al., 2008; Hauri et al., 2011, 2015). The total amount of CO, a mass fraction $n_{COt}$, would have predominantly been formed over a narrow (< 1 MPa) pressure interval as the magma passed through the 40 MPa level (Nicholis and Rutherford, 2009), at a depth of ~9.7 km in a lunar crust with density 2550 kg $m^{-3}$ (Wieczorek et al., 2013) assuming that the pressure distribution in the rising magma was close to lithostatic, a necessary assumption since the dike and conduit system was stable. Water would have been exsolved at much lower pressures, for example at ~0.9 MPa (corresponding to ~220 m depth) if the water content were 1000 ppm and the water solubility in lunar basalt were similar to that in terrestrial mafic magma (Dixon, 1997), approximated by:

$$n_{H2Od} = 6.8 \times 10^{-8} P^{0.7} \quad (1),$$

where $n_{H2Od}$ is the water solubility given as a mass fraction when $P$ is in Pascals. In general, if the total amount of pre-eruption water was $n_{H2Ot}$, then the amount exsolved at pressure $P$ would be $n_{H2Oe}$ where

ACCEPTED MANUSCRIPT


$$n_{H2Oe} = n_{H2Ot} - n_{H2Od} \quad (2),$$

noting that if $P$ is greater than the saturation pressure given by equation (1) for the chosen $n_{H2Ot}$, then $n_{H2Oe}$ is zero.

At the high strain rates typical of steady explosive activity, the rising magma would have fragmented when the bubble volume fraction had increased to a critical value of ~75-80 volume % (Mader et al., 1994; Mangan and Cashman, 1996). The pressure, $P_{frag}$, at which this occurred can be found by evaluating the partial volume fractions of the gas and magmatic liquid. At magmatic temperatures and pressures up to tens of MPa the properties of both gases can be approximated by the ideal gas law, and so the specific volume fractions of total released gas, $v_g$, and liquid magma, $v_m$, are given in general by

$$v_g = [(Q\ T) / P]\ [(n_{H2Oe} / m_{H2O}) + (n_{COt} / m_{CO})] \quad (3a),$$

$$v_m = (1 - n_{H2Oe} - n_{COt}) / \rho_m \quad (3b),$$

where $Q$ is the universal gas constant, equal to 8.314 kJ kmol$^{-1}$ K$^{-1}$, $T$ is the magma temperature, taken as 1500 K, $m_{H2O}$ and $m_{CO}$ are the molecular masses of $H_2O$ and CO, 18.015 and 28.010 kg kmol$^{-1}$, respectively, and $\rho_m$ is the density of the magmatic liquid, ~3000 kg m$^{-3}$. The gas volume fraction, $f_g$, in the bulk liquid-gas mixture, i.e. the vesicularity, is

$$f_g = v_g / (v_g + v_m) \quad (4).$$

The requirement that $n_{H2Oe}$ must not be negative means that these equations cannot be readily rearranged analytically to give $P$ as a function of the other variables. Instead, a spreadsheet can be used to evaluate $f_g$ for any chosen set of values of $P$, $n_{COt}$ and $n_{H2Ot}$. $P$ is varied by trial and error until $f_g$ is equal to the vesicularity at which magma fragmentation is expected to occur, at which point $P$ is equal to $P_{frag}$.

If we take CO and water contents in the middle of the likely ranges for the Moon, say 1000 ppm CO and 500 ppm $H_2O$, vesicularities of 75 and 80% will be reached at fragmentation

ACCEPTED MANUSCRIPT


pressures of $P_{frag}$ = 0.431 and 0.327 MPa, respectively, corresponding to depths below the surface of 104 and 79 m. The higher of these pressures is greater than the water saturation pressure of 0.334 MPa for 500 ppm $H_2O$ in basalt, and so water release would only have occurred after the magma had fragmented due to CO bubble expansion, potentially leading to a second stage of water-driven magma fragmentation. The primary fragmentation due to CO bubble expansion would have produced pyroclasts whose typical size would have been dictated by the growth by decompression of bubbles nucleating at 40 MPa pressure with diameters of ~20 microns (Sparks, 1978). With fragmentation at 0.431 MPa, the bubble diameters would have increased to $[(40/0.431)^{1/3} \times 20 =]$ 90.5 microns, producing pyroclasts with a similar size. If fragmentation were delayed until 0.327 MPa (depth of 79 m) the corresponding typical size would have been 99.3 microns.

The explosive activity generated by these scenarios would have involved fire fountains in which the sub-millimeter sized clasts would have had initial eruption speeds essentially equal to the speed of the expanding gases, $u_g$. Decoupling between expanding gas and accelerating clasts would occur when the mean free path between gas molecule collisions exceeded the size of the clasts, in the so-called Knudsen regime, at a pressure $P_d$ given by

$$P_d = (2^{1/2}\, Q\, T) / (3\, \pi\, \phi^2\, N_a\, d) \qquad (5),$$

where $\phi$ is the effective diameter of the gas molecules ($\phi_{CO}$ = ~3.4 ×$10^{-10}$ m, $\phi_{H2O}$ = ~3.8 ×$10^{-10}$ m), $N_a$ is Avogadro's number, 6.0225 ×$10^{26}$ $kmol^{-1}$, and $d$ is the mean clast diameter. For typical $d$ = ~90-100 μm sized pyroclasts, $P_d$ is ~250 Pa. The final speeds of the pyroclasts can then be found by equating the kinetic energy of the products to the energy released by the gas expansion:

$$0.5\, u_g^2 = Q\, T\, [(n_{H2Oe} / m_{H2O}) + (n_{COt} / m_{CO})]\, \ln\, (P_{frag} / P_d) \qquad (6).$$

For a mixture of 1000 ppm CO and 500 ppm $H_2O$ the eruption speed is $u_g$ = ~81 m $s^{-1}$. The maximum pyroclast range, $R$, implied by this speed is ($u_g^2$ / $g$), where $g$ is the acceleration due to gravity, 1.62 m $s^{-2}$, and in this case is very close to 4 km.

The small (sub-mm) average pyroclast sizes would have caused the central part of the fire fountain over the vent to be optically dense so that all of the pyroclasts landing from this part of

ACCEPTED MANUSCRIPT


the fountain reached the ground at magmatic temperatures and coalesced to form a lava lake that overflowed to feed the lava flows that formed the small shield volcano (Figs. 2b-2c) (Head and Wilson, 2016; their Fig. 19). The lake is interpreted to be represented by the present size of a sample shield volcano summit depression: we use the Ina small shield and summit pit crater (Fig. 1a), which has a radius of ~1500 m (Garry et al., 2012), near the upper range of shield volcano pit diameters (Head and Gifford, 1980). Since the maximum range of pyroclasts was ~4 km, this implies that the optically thin outer shell of the fire fountain, from which heat was able to escape by radiation into space, had a thickness, *S*, of ~(4000 - 1500 =) 2500 m. Fire-fountain structures of this type have been modeled by Wilson and Keil (1997, 2012) and Wilson and Head (2001). Wilson and Head (2016) made some additions to the earlier treatments and showed that for point-source vents (as distinct from elongate fissure vents), *S* is best approximated by

$$S = (6.17\, d\, g^{1/2}\, R^{5/2}) / V \qquad (7),$$

where *V* is the dense rock equivalent erupted volume flux. For *S* = 2500 m, *d* = 95 μm and *R* = 4000 m, *V* is found to be ~380 $m^3\ s^{-1}$.

The above analysis has been repeated for a wide range of values of the assumed CO and water contents of lunar magma, and Table 1 shows the results. As noted earlier, depending on the CO and water contents of the magma, fragmentation due to CO expansion may occur before any water release, and so for each chosen CO content there will be a water content below which there is no change in the eruption speed and maximum pyroclast range - these values are indicated in the table. Furthermore, there will be some combinations of CO and water content for which the implied maximum range of pyroclasts is less than the radius of the shield volcano summit depression, and clearly such combinations cannot explain the size of the depression in terms of the model proposed here. All of the volatile combinations shown in Table 1 are capable of explaining the size of the depression, though only just so in the case of the smallest volatile content permutations. Taken together, the values in the table suggest that it is unlikely that the water content of the magma erupted at Ina, among the largest shield volcano summit pits, was less than ~300-400 ppm.

The magma volume flux feeding the steady explosive part of the eruption can be estimated not only from the fire fountain geometry but also from the radial extents of the flows forming the

ACCEPTED MANUSCRIPT


shield by assuming that they were cooling limited. Pinkerton and Wilson (1994) found that flows of mafic lavas stopped advancing as a result of cooling when the dimensionless Grätz number describing their motion decreased from an initially large value as the flow left the vent to a final critical value close to 300. Wilson and Head (2016) showed that a suitable version of the relationship for channelized flows in terms of directly-measurable parameters is

$$V = (18.75\ \kappa\ X\ W) / Z \qquad (8),$$

where κ is the thermal diffusivity of lava, ~$10^{-6}$ $m^2$ $s^{-1}$, and *W*, *X* and *Z* are the flow width, length and thickness, respectively. The average radius of the shield is ~12 km (Garry et al. 2012; Qiao et al., 2016a) and we adopt this value for *X*. The average slope of the flanks of the shield is ~ 0.03. Mare basalts emplaced on slopes of ~0.001 in Mare Imbrium have thicknesses of ~30 m, and lava flow thickness is proportional to the apparent yield strength of the material forming the lava flow levees (Hulme, 1974). If the flows on the Ina shield have similar yield strengths to the Imbrium flows we can expect their thicknesses to be about [(0.001 / 0.03) × 30 =] one meter. It is difficult to estimate the widths of these flows, but irregularities in the dome margin suggest a value of ~1000-2000 m. These values yield an estimate of $V$ = 225 to 450 $m^3$ $s^{-1}$, a range that brackets most of the of volume fluxes derived from the fire fountain model in Table 1 except those from the largest assumed CO content. Thus if the 225 to 450 $m^3$ $s^{-1}$ range is regarded as reliable, it implies that the CO content of the magma at the Ina example was not much greater than 1000 ppm. However, it is clearly plausible that more than one lava flow was being fed from the lava lake at any one time, and so higher volatile contents, up to the maximum values estimated for mare basalts shown in Table 1, and higher volume fluxes, up to at least ~800 $m^3$ $s^{-1}$, are also possible.

**4. Strombolian explosive phase**

As the volume flux declined towards the end of the eruption, the rise speed of the magma everywhere in the dike decreased and it became more and more likely that CO bubbles would have had time to coalesce as they formed and ascended through the uppermost ~10 km of the rising magma (Figs. 2c-2d). This would have led to a change in eruption style towards strombolian activity (Figs. 2d, 3), in which large CO bubbles would have emerged intermittently

ACCEPTED MANUSCRIPT


through the surface of a lava lake. These bubbles would have updomed the lava surface, and clots of the fragmented skin of the bubbles would have been ejected as pyroclasts as the bubbles burst (Fig. 3, left text). Loss of magma from the vent to form these pyroclasts would have been compensated by the slow rise of magma through the dike and near-surface conduit into the lake, and $H_2O$ gas bubbles would have continued to nucleate in the rising magma as it neared the surface. We have no direct evidence of the shape of the conduit through which the eruption took place, but we can present some possible options for this stage.

We predict that in the late stages of this eruption the volume flux had decreased from the value feeding the fire fountain stage by at least an order of magnitude, say $V = 35$ m$^3$ s$^{-1}$. Wilson and Head (2016) showed that the typical pressure gradient, $P'$, driving vigorous eruptions from deep magma sources on the Moon would be ~185 Pa m$^{-1}$. If we assume that the late stages of the eruption occur with a gradient, like the magma volume flux, about an order of magnitude smaller we can adopt $P' = 20$ Pa m$^{-1}$. Finally, for lunar basalts we can take $\eta = 0.5$ Pa s (Section 6.1.1 in Taylor et al., 1991).

Assume first that the conduit is a circular tube of radius $r$. The rise speed is then $u_m$ where

$$u_m = (P' r^2) / (8 \eta), \quad \text{for laminar magma motion} \quad (9a),$$

$$u_m = [(r P')/(f \rho_m)]^{1/2} \quad \text{for turbulent magma motion} \quad (9b),$$

and $f$ is a wall friction factor of ~ 0.02. The corresponding volume flux, $V$, is ($u_m \pi r^2$), i.e.

$$V = (\pi P' r^4) / (8 \eta) \quad \text{laminar case} \quad (10a)$$

$$V = \pi r^{5/2} [P' / (f \rho_m)]^{1/2} \quad \text{turbulent case} \quad (10b)$$

Since we do not know in advance which solution is relevant in any given case we evaluate both pairs of equations; whichever solution yields the smaller velocity is the correct one (Wilson and Head, 1981). With the above values of $P'$, $\eta$, $f$ and $\rho_m$ we find that the turbulent flow solution is the relevant one, with $r = 3.3$ m, $u_m = 1.0$ m s$^{-1}$.

ACCEPTED MANUSCRIPT


The asymmetry of the Ina depression (Fig. 1a) suggests that the conduit may not be circular but instead may retain some of the geometry if its original dike/fissure structure. If so, it should be treated as an elongate shape of length $F$ and width $w$. The initially opened dike would have had a shape controlled by the elastic properties of the host rock, such that the aspect ratio $A = F / w$ would have been of order 1000. Progressive cooling of magma in the dike as the eruption waned would have preferentially sealed the outermost, thinnest parts of the dike, reducing the ratio $A$ to perhaps 100 or even as little as 10. The equivalents of the above equations for magma rise speed and volume flux in the elongate shape case are

$$u_m = (P' w^2) / (12 \eta), \quad \text{for laminar magma motion} \quad (11a),$$

$$u_m = [(w P')/(f \rho_m)]^{1/2} \quad \text{for turbulent magma motion} \quad (11b),$$

$$V = (A P' w^4) / (12 \eta) \quad \text{laminar case} \quad (12a)$$

$$V = A w^{5/2} [P' / (f \rho_m)]^{1/2} \quad \text{turbulent case} \quad (12b).$$

In all cases the solutions are found to be fully turbulent. For $A = 100$ the solutions are $F = 82$ m, $w = 0.82$ m, and $u_m = 0.52$ m s$^{-1}$. For $A = 10$, the solutions are $F = 20.6$ m, $w = 2.06$ m, and $u_m = 0.83$ m s$^{-1}$.

The common factor in the above solutions is that they all lead to magma rise speeds close to or less than ~1 m s$^{-1}$. We need to consider if this result is consistent with the strombolian activity that we have postulated. Strombolian activity is assumed to most commonly ensue from coalescence of gas bubbles in magma, which has time to occur when the average rise speed of the bubbles in the liquid magma is comparable to the rise speed of the magma through the volcanic conduit system (Figs. 2d, 3). The mechanics of this process were modeled by Parfitt and Wilson (1995) for basaltic magmas on Earth exsolving $H_2O$. They found that to allow efficient coalescence to occur the magma rise speed needed to be less than a critical value that was a strong function of the magma water content and a weak function of the magma viscosity. For a water content of 1 wt % the critical speeds were 0.2, 0.1 and 0.05 m s$^{-1}$ for viscosities of 30, 100 and 300 Pa s, respectively. For a water content of 0.5 wt % the corresponding speeds

ACCEPTED MANUSCRIPT


were 0.1, 0.04 and 0.02 m $s^{-1}$, and for a water content of 0.25 wt % they were 0.025, 0.01 and 0.004 m $s^{-1}$. The key issue is the time available for the bubbles to interact. With 1 wt % water, bubbles first nucleated at a depth of ~840 m; with 0.5 and 0.25 wt% the corresponding depths were 310 and 110 m, respectively. Dividing the depths over which bubble coalescence occurred by the critical rise speeds yields average magma travel times of at least 3650, 8240 and 21360 seconds for magma viscosities of 30, 100 and 300 P as, respectively: the time is proportional to the viscosity raised to the power 0.766. Using this relationship, the critical time corresponding to a lunar magma viscosity of 0.5 Pa s would be ~160 seconds. In the lunar case we are dealing with CO generated abruptly at the 40 MPa level at a depth of ~9.7 km, so magma taking 160 s to travel 9.7 km would be moving at ~61 m $s^{-1}$. However, bubble rise speeds in magma are inversely proportional not only to the magma viscosity but also to the acceleration due to gravity, so to allow efficient bubble coalescence in a 0.5 Pa s lunar magma the rise speed should be less than [(1.62 / 9.8) × 61 =] 10 m $s^{-1}$. Since our scenarios above for late-stage eruptive activity at Ina all have magma rise speeds less than ~1 m $s^{-1}$ it would be very surprising if strombolian activity (Fig. 3) did not occur.

An important consequence of the strombolian activity phase is that it allows a cooled crust to form on a lava lake (Fig. 3, right text). During the hawaiian phase, the great optical density of the fire fountain allows pyroclasts in its core to remain hot. At very high mass fluxes essentially all of the pyroclasts will coalesce into lava flows as they reach the surface and no localized lake is present. At somewhat lower mass fluxes the outer part of the fountain will consist of partly-cooled clasts that form a spatter deposit allowing an overflowing lava lake to form around the core of the fountain, but radiation from the surface of the lake will still be inhibited by the cloud of pyroclasts above it. However, once strombolian activity dominates, a stable lake is likely to be present and radiative cooling begins. There is additional cooling of the magma clots thrown up from the bursting of the CO bubbles through the lake surface. Ejecta from strombolian explosions on Earth have sizes spanning the centimeter through decimeter to meter range (Self et al., 1974; Gaudin et al., 2014) and since the clast sizes are dictated mainly by the response of the cooled lava lake surface layer to sudden deformation by large bubbles, we expect similar sizes in lunar events provided the lake crust has grown in thickness to depths of this order. The very largest clasts may not be significantly accelerated by the expansion of the gas released from the bursting bubbles and their speeds will be similar to those of the rising bubbles. Since we expect

ACCEPTED MANUSCRIPT


dike widths, *w*, in the range ~30 to ~150 m (Wilson and Head, 2016), the rise speeds of large bubbles essentially filling the conduits will be ~0.34 $(w\,g)^{1/2}$ (Viana et al., 2003), i.e., ~2.4 to ~5.3 m $s^{-1}$ implying clast ranges of only ~3 to 17 m. However, decimeter-sized clasts observed in strombolian explosions on Earth have speeds of many tens of m $s^{-1}$ (Self et al., 1974; Blackburn et al., 1976; Gaudin et al., 2014), and this can be ascribed to the initial trapping of expanding gas until sufficient gaps between clasts have developed to allow gas escape (Self et al., 1979), as occurs in vulcanian explosions. Models developed for vulcanian eruptions on Mars (Fagents and Wilson, 1996), where the atmospheric pressure is very low, show that speeds up to 120 m $s^{-1}$, implying ranges up to nearly 9 km, are readily attainable for the gas-to-ejecta mass ratios in lunar strombolian explosions. The clots of ejected lake surface magma will themselves be very vesicular on a millimeter and smaller scale, as we show below. Their disruption and random reassembly as they fall back into the cooling lake surface (Fig. 3) will lead to a macroscopic porosity on a similar scale to that of the clast size. It is therefore important to establish the thickness reached by the lava lake crust during the period of strombolian activity at Ina.

We estimate the thickness by considering the likely duration of the hawaiian and strombolian phases of activity. The volume of the Ina shield can be estimated from the topographic data in Garry et al. (2012) and Qiao et al. (2016a) to be ~79 $km^3$. The edifice is built from vesicular lava and loosely packed pyroclastics and has a height above the surrounding surface of ~300 m. Under lunar gravity this means that the pressure at the base of the pile is at most ~1.3 MPa. We therefore assume that it has on average a porosity of ~30%, implying a dense-rock equivalent volume of ~55 cubic $km^3$. The upper end of the volume flux estimates found above for the hawaiian phase of the eruption was ~800 $m^3\ s^{-1}$; this implies that if all of the edifice was built during the hawaiian phase the duration of that activity was at least $6.9 \times 10^7$ s, i.e. ~2.2 years. In practice, some of the edifice must have been constructed during the strombolian activity phase as the eruption was ending. Strombolian activity requires that the rise speed of the magma be significantly reduced to allow time for bubble coalescence to occur in the rising magma, and a lower magma rise speed implies a lower magma volume flux. As an illustration we can assume that most of the edifice was constructed during the hawaiian phase, say 54 $km^3$ constructed at 800 $m^3\ s^{-1}$ for 2.1 years, with the remaining 1 $km^3$ constructed during the strombolian phase at 80 $m^3\ s^{-1}$, an order of magnitude reduction in eruption rate, requiring

ACCEPTED MANUSCRIPT


~0.4 years. The thickness, $C$, of the solid crust on a lava lake that has been cooling for a time $t$ is given approximately (e.g., Section 4-18 in Turcotte and Schubert, 2002) by

$$C = 1.75\ (\kappa\ t)^{1/2} \qquad (13)$$

and with $t$ = 0.4 years, $C$ = ~6.2 m. Clearly other eruption histories can be constructed. However, to be consistent with the various constraints imposed by the morphology of the Ina depression and its host shield volcano, the time scales could not be different from this one by more than a factor of order two. The duration of the strombolian phase must have been of order several months leading to a crust thickness of order several meters (Fig. 3).

## 5. Foam formation and extrusion stage

### *5.1. Foam stabilization in the lava lake*

The final stage of the eruption occurs when the magma rise speed at great depth becomes vanishingly small. No further CO is produced because no magma is passing through the 40 MPa level, and a final slug or giant bubble of CO emerges at the surface in a final strombolian explosion (Figs. 2d, 3, left text). The dike is now relaxing elastically as the excess pressure in the magma vanishes and residual dike magma is squeezed slowly up towards the surface (Figs. 2e-2f). At the top of the magma column is the crust consisting of coarse pyroclastic material of a range of sizes that fell back into the vent during the strombolian phase and otherwise of magma that cooled into the overlying vacuum (Fig. 3, right text). Bubbles of water vapor that had nucleated in the magma entering the lava lake will have expanded as a result of decompression (Fig. 4). Bubbles will also grow by continued diffusion of $H_2O$ molecules through the magmatic liquid, and larger bubbles will grow at the expense of smaller ones with which they are in contact by the process of Ostwald ripening (Mangan and Cashman, 1996). Now that it is no longer being subjected to intermittent shearing by the large CO bubbles this foam forms a stable layer (Figs. 2e, 4).

The crust overlying the foam will be subjected to tensile stresses by both cooling and the addition to the lake of magma forced out of the underlying dike (Figs. 2f, 4). Silicate rocks subject to a few hundred degrees of cooling can experience tensile stresses in excess of their tensile strengths (Savage, 1978), and this may have initiated fractures propagating downward

ACCEPTED MANUSCRIPT


from the surface of the crust. The global cooling of the Moon in the latter half of its volcanic history (younger that ~3.5 billion years; Head and Wilson, 2016) generated compressive stresses of at least tens of MPa (Solomon and Head, 1980) in the lunar crust that, acting on the dike walls and being communicated through the magma column into the lava lake, would have exerted similar stresses on the base of the lava crust. Thus it seems inevitable that fractures will form in the crust through which the underlying foam can be extruded out onto the surface to form the mounds visible on the floor of the Ina depression (Figs. 4, 5).

It is possible that bubbles in the top of the foam in these fractures will explode in a mini-strombolian fashion (Fig. 5). These bubbles have gas at a finite pressure on one side of the liquid film forming the upper bubble wall but have a hard vacuum on the other side. This tendency will be resisted by capillary forces controlled by the surface tension of the magma, $\sigma$, ~0.37 J $m^{-2}$. Specifically, the bubbles will be able to avoid rupture as long as the gas pressure inside them is less than a critical value, $P_c$, given by Mangan and Cashman (1996) as

$$P_c = [(4\,\sigma) / \varphi] \qquad (14)$$

where $\varphi$ is the bubble radius. The internal pressure and bubble size can be found by solving equations (1) through (4) with only water vapor present. A recursive method in a spreadsheet is again used to solve for the gas pressure, $P$, in the bubbles as a function of the chosen values of pre-eruption water content, $n_{H2Ot}$, and magma temperature and density. It is again necessary to decide what volume fraction of the magmatic foam is likely to consist of gas in the present conditions, where the slowly rising magma is not subjected to large shearing forces but is erupting into a vacuum. In a series of experiments in which melted samples of terrestrial basalts were exposed to progressively lower pressures in a vacuum system, Fielder et al. (1967) found that vesicularities of up to 94% were produced. This is comparable to the vesicularities of up to 96% in reticulite clasts from basaltic eruptions measured by Mangan and Cashman (1996). Bubble sizes in the experimental foams were mainly in the range 100-1000 $\mu$m, and some bubble bursting occurred as the pressure decreased below ~3 kPa. These findings are in good agreement with equation (14). We adopt a vesicularity of 95%, i.e. $f_g = 0.95$, which corresponds to a foam bulk density, $\rho_f$ = 150 kg $m^{-3}$, and find the pressure, $P_f$, that leads to this vesicularity in the foam for water contents of 1000, 500 and 250 ppm. We then find the water vapor bubble radius, $r_f$, at

ACCEPTED MANUSCRIPT


the pressure $P_f$ on the assumption that the bubble expanded to this pressure after nucleating with a radius of 10 μm (Sparks, 1978) at a pressure $P_n$ given by equation (1) for the assumed total water content $n_{H2Ot}$. Finally, the capillary pressure, $P_c$, that will resist bubble bursting for the final bubble radius $r_f$ is found from equation (13). If $P_c$ is greater than $P_f$ the foam is stable. If the reverse is true, the foam is not stable against exploding into the overlying vacuum, but will become stable after a sufficient thickness of pyroclastic debris has accumulated above it (Fig. 5). The thickness of this layer, $D_p$, can be found by dividing the pressure that it must exert, $(P_f - P_c)$, by its density, $\rho_c$, and the acceleration due to gravity, $g$. The bulk density of the loosely-packed accumulating pyroclasts will depend on the particle size distribution and packing efficiency but is likely be about two thirds that of the magma, say $\rho_c = 2000$ kg m$^{-3}$.

Table 2 shows the results of this analysis. For water contents less than ~830 ppm, a 95% vesicular foam is stable. For somewhat greater water contents in the range likely to be relevant to lunar basalts, the foam can be made stable by the addition of a layer of loose pyroclasts with thicknesses of order decimeters to a few meters (Fig. 5). Of course, radiative cooling of the free surface of an uncovered foam quite quickly leads to enhanced stability of the outer layers as the liquid magma solidifies. A final configuration is clearly possible in which what was previously the heterogeneously vesicular liquid lava lake at the summit of the Ina shield, stirred and disrupted by large escaping CO gas bubbles, evolved at the end of the strombolian phase into a layer of extremely vesicular and stable foam extending down into the upper part of the vent and conduit system to a depth, $D_f$, at which no further water vapor bubble nucleation occurred (Figs. 2e, 4). $D_f$ is found by evaluating the bulk density of the foam, $\rho_f$, at the surface and finding the pressure increase $\delta P = \rho_f g \delta D_f$ under a thin layer of depth $\delta D_f$ with this density. The amount of water vapor exsolved at this new pressure is found and the new density at this new depth is evaluated so that the next pressure increment can be found. This numerical integration is continued downward until the pressure becomes equal to the water nucleation pressure, at which point no more water is exsolved and the vesicularity becomes zero. Table 2 shows that, for the 250-1000 ppm range of water contents likely to be relevant to lunar magmas, a foam layer could have vertical extent between 100 and 700 m (Fig. 2e). Foam would be lost from the top of this layer by erupting through cracks in the crust (Figs. 4, 5) and replenished from below until either the feeder dike was completely relaxed or magma in the shallow conduit cooled to solidification (Fig. 4).

ACCEPTED MANUSCRIPT


*5.2. Foam extrusion through lake crust*

The profiles of the Ina depression shown in Fig. 3(c) of Garry et al. (2012) and in Qiao et al. (2016a) suggest that the lava lake was deeper in the center than at the edges. Thus as the broken lake crust subsided, significant gaps must have appeared between broken crustal plates, allowing foam extrusion. This can be modeled by assuming that the eruption of foam to form mounds is exactly matched by crustal plates sinking due to their negative buoyancy. Any addition of foam from the dike into the base of the lake after mound formation initiates will cause some uplift of the crust together with the mounds perched on top of it, but this does not significantly influence the results found from the following calculation. Assume that the crust is broken into plates of typical horizontal size $L$ and thickness $Y$; for simplicity it is assumed that the plates are all equal-sized squares of side $L$. There is a gap between adjacent plates of width $G$. As before, the density of the material forming the plates is $\rho_c$ and the density of the foam rising though the gaps is $\rho_f$. The downward sinking speed of each plate is $U_P$ relative to a fixed datum and the rise speed of the foam relative to the walls of the gap is $U_F$. As a result the rise speed of the foam relative to a fixed datum is $(U_F - U_P)$. The volume flux represented by the sinking of any one plate is $(L^2 U_P)$. Each plate has four sides shared with adjacent plates. The downward volume flux of the plate is balanced by half of the volume flux rising through each of the four gaps along its edges (the other half contributing to the compensation for the adjacent plate), and so the total upward compensation flux from the four gaps is four contributions of $[0.5 G L (U_F - U_P)]$. Equating the volume fluxes and simplifying,

$$U_F = U_P [1 + 0.5 (L / G)] \quad (15)$$

Based on the measured separations of a random selection of mounds, we estimate $L$ to average 150 m. The widths of the gaps between mounds cannot be estimated from images because the gaps are narrow and generally buried. However, we can estimate a typical value by assuming that the gaps represent the lateral separation of crustal plates as they subside. The cross-sectional profile of Ina shows that the envelope of the tops of the mounds is approximately

ACCEPTED MANUSCRIPT


the lower half of an ellipse with semi-major (horizontal) axis, *a*, equal to half of the width of the pond, ~1300 m, and semi-minor (vertical) axis, *b*, equal to the depression in the middle of the pond, ~20 m. The longer semi-perimeter *s* of an elongate ellipse of this shape is given (Ramanujan, 1914; Michon, 2015) by

$$s = 0.5\ \pi\ [2 - (7 / 22)\ \pi]\ (a + b)\ \{1 + [(3\ h) / (10 + (4 - 3\ h)^{1/2})]\} \quad (16)$$

where

$$h = [(a - b) / (a + b)]^2 \quad (17)$$

which leads to $s$ = 2602.956 m, to be compared with the linear dimension of the crust, 2600 m. Thus the ratio ($G$ / $L$) = (2.956 / 2600) = 0.001137 and with $L$ = 150 m, $G$ = ~0.17 m.

Very vesicular foams are expected to have a non-Newtonian rheology. Dollet and Raufast (2014, their Fig. 5) show that a 95% monodisperse foam would be expected to have a yield strength, $\tau_y$, controlled by surface tension and typical bubble radius such that

$$\tau_y = K\ (\sigma / \varphi) \quad (18).$$

where for a 95% foam $K$ = 0.055. We estimated earlier (Table 2) that the stable foam emplaced in the lava lake would have contained bubbles with radii $\varphi$ = ~20 μm, which would imply that $\tau_y$ was ~1000 Pa. If a material with a yield strength rises through a parallel-sided channel, the flow consists of a zone of shearing fluid on either side of a central plug of width $W_{plug}$ given by

$$W_{plug} = (2\ \tau_y) / [g\ (\rho_p - \rho_f)] \quad (19)$$

where $\rho_p$ is the density of the sinking plate, $\rho_f$ is the density of the rising foam and [$g$ ($\rho_p$ - $\rho_f$)] is the pressure gradient driving the flow. A 95% vesicular foam in a lunar magma of density 3000 kg m$^{-3}$ will have a bulk density of $\rho_f$ = 150 kg m$^{-3}$, and a crustal plate derived from this foam that has lost, say, half of its vesicularity during its development will have a density of $\rho_c$ = 1575 kg m$^{-3}$, so ($\rho_p$ - $\rho_f$) will be ~1425 kg m$^{-3}$. With this value and $\tau_y$ = 1000 Pa, equation (19) implies

ACCEPTED MANUSCRIPT


that $W_{plug}$ = ~0.87 m, which is greater than the width $G$ = ~0.17 m of the crack through which the foam is rising. Clearly the effective yield strength of the foam must be much less than 1000 Pa, and in the context of the Dollet and Raufast (2014) treatment this implies that the typical gas bubble size in the foam must be much larger than $\varphi$ = ~20 μm. As an example, if the plug filled half of the crack width, $\varphi$ would need to be ~200 μm. The time needed for the crust on the lava lake to acquire a thickness of at least 3-4 meters, as evidenced by the size of boulders and general roughness on its surface, and develop major fractures is ~2-3 months. It seems likely that during this period a combination of bubble coalescence and Ostwald ripening could readily have produced the increase of typical bubble size required.

In order to explore the range of possible conditions controlling the escape of foam through the cracks in the crustal plate we define the ratio, $q$, of the size of the central plug to the width of the crack:

$$q = W_{plug} / G \qquad (20).$$

In terms of this parameter, the speed, $U_{plug}$ of the central plug rising through the crack is given by (Skelland, 1967):

$$U_{plug} = [(1 - q^2)\, G^2\, g\, (\rho_p - \rho_f)] / (8\, \eta_B) \qquad (21),$$

where $\eta_B$ is the plastic viscosity of the Bingham material. The bulk velocity of the foam, $U_F$, including both sheared fluid and plug is

$$U_F = [(2 + q) / 3]\, U_{plug} \qquad (22)$$

The ratio $q$ must, by definition, lie between zero and unity, so Table 3 shows, as a function of $q$, the values of $W_{plug}$ from equation (20), $\tau_y$ from equation (19) and $\varphi$ from equation (18). The values of $\tau_y$ are mainly within a factor of 3 of 50 Pa s. To go further we require a value for the plastic viscosity, $\eta_B$. There are many values in the literature for the rheological parameters of mafic lavas treated as Bingham plastics, but these commonly relate to lavas forming flows well away from the vent after significant cooling. In the present case we have a lava foam well

ACCEPTED MANUSCRIPT


insulated by an overlying crust. Based on data for lavas close to their vents merged with sub-liquidus laboratory measurements by Ishibashi and Sato (2010), Fig. 13 of Wilson and Mouginis-Mark (2014) shows that for a mafic lava with $\tau_y$ = 50 Pa we would expect $\eta_B$ to be ~500 Pa s. Using this estimate we can then add to Table 3 the values of $U_{plug}$ from equation (21) and $U_F$ from equation (22) and $U_P$ from equation (15). Finally, the average volume flux, $E$, of foam feeding a typical mound can found by multiplying the foam rise speed $U_F$ by the length $L$ and width $G$ of a gap and noting that, given our assumed regular square geometry, any one mound is fed on average by half of the volume flux from each of the four gaps that meet beneath it:

$$E = 2\, U_F\, L\, G \qquad (23)$$

Typical values from Table 3 are a foam rise speed of ~11 mm $s^{-1}$, a plate sinking speed of ~13 μm $s^{-1}$, and an erupted volume flux of 0.6 $m^3$ $s^{-1}$. The depression of the center of the Ina lake is ~20 m and so the average crustal plate subsided by ~10 m; the time, $t_e$, needed for this to occur would have been (10 m / 13 μm $s^{-1}$ =) about 9 days. With an average foam volume flux of 0.6 $m^3$ $s^{-1}$ a typical mound volume should therefore be ~$4.6 \times 10^5$ $m^3$. The measured volumes of the 85 identified mounds on the floor of Ina total 0.0258 $km^3$ (Qiao et al., 2016a); there is a very wide range of individual mound volumes, the maximum and minimum values being $9.2 \times 10^6$ and 41 $m^3$, respectively. The mean and median values of the skewed distribution are $3.0 \times 10^5$ and $1.6 \times 10^4$ $m^3$, respectively. The measured mean of $3 \times 10^5$ $m^3$ is somewhat smaller than the $4.6 \times 10^5$ $m^3$ value estimated from the dynamic analysis; however, given the many uncertainties in both the densities and the foam viscosity, the agreement is considered satisfactory.

*5.3. Formation of mounds as foam lava flows*

The availability of high-resolution topographic data, as well as imaging data, for the interior of the Ina depression enables us to model the emplacement of the mounds on the floor. The topography of one of the mounds, emanating from an inclined part of the lake crust close to an inner wall of the depression, is shown in Figure 6. We continue to treat the rheology as Bingham plastic with yield strength $\tau_y$ and plastic viscosity $\eta_B$ and adopt the model proposed by Hulme (1974) for the morphology of lava flows with this rheology. The model assumes that motion occurs in a channel of central depth $D_c$ and width $W_c$ contained between stationary

ACCEPTED MANUSCRIPT


levées, each of which has a width $W_b$ and a maximum thickness $D_b$ where it abuts the central channel. It can be shown that if $\alpha$ is the slope of the substrate over which the flow is moving,

$$D_b = \tau_y / (\rho\, g \sin \alpha) \quad (24),$$

$$W_b = \tau_y / (2\, \rho\, g \sin^2 \alpha) \quad (25),$$

$$D_c = [(W_t\, \tau_y) / (\rho\, g)]^{1/2} \quad (26),$$

where $W_t$ is the total width of the flow,

$$W_t = W_c + 2\, W_b \quad (27).$$

Hulme (1974) showed that the width of the central channel within which lava moves, $W_c$, can be related to the erupted volume flux, $E$, the slope of the substrate, $\alpha$, and the material properties of the lava. The relationship can be expressed as

$$W_c = [(24\, E\, \eta_p) / (\tau_y \sin^2 \alpha)]^{1/3} \quad , W_c / (2\, W_b) \leq 1 \quad (28a),$$

$$W_c = [(24\, E\, \eta_p)^{4/11}\, (\rho\, g)^{1/11}] / (\tau_y^{\,5/11}\, \sin^{6/11} \alpha) \quad , W_c / (2\, W_b) \geq 1 \quad (28b).$$

These equations represent good approximations to Hulme's (1974) original expression, which involved a single polynomial in the quantity $[W_c/(2\, W_b)]$, and were introduced by Wilson and Head (1983) to make it possible to invert the equation and solve analytically for $W_c$. In any given case it is necessary to evaluate both expressions and chose whichever yields the self-consistent solution.

In the present case we can measure $\alpha$ from the topographic data, and $D_c$ and $W_t$ from the imaging data. The slope over the proximal 50 m of the flow, before it begins to pond on a shallower part of the floor of the depression, is sin $\alpha$ = ~0.065. The part of the flow on this slope has a thickness of $D_c$ = ~6 m and is about $W_t$ = 115 m wide. If the flow is a 95% foam, its

ACCEPTED MANUSCRIPT


density $\rho$ = 150 kg m$^{-3}$, and for the Moon $g$ = 1.62 m s$^{-2}$. Then equation (26) gives $\tau_y$ = 89.3 Pa, and equation (24) gives $D_b$ = 5.65 m. Note the reality check that $D_b$ is less than $D_c$, as it must be. Next, equation (25) gives $W_b$ as 43.5 m and equation (27) gives the width of the flowing central channel, $W_c$, as (115 - 2 × 43.5 =) 28 m. Since $W_c$ is less than (2 $W_b$), equation (28a) is the appropriate choice to find the product ($E$ $\eta_B$); the value is 347 Pa m$^3$. Earlier we suggested that the plastic viscosity of the foam was expected to be of order 500 Pa s; this would imply an effusion rate of 0.69 m$^3$ s$^{-1}$. This effusion rate is very similar to the 0.57 m$^3$ s$^{-1}$ estimated earlier, and would imply that this entire flow unit, which has a volume of ~6.21 × 10$^5$ m$^3$, making it one of the largest mounds, was emplaced over a time period, $t_e$, of ~10 days.

Given that there is considerable uncertainty in estimating the thickness of the flow and the slope on which it formed, we investigate the sensitivity of the effusion rate to the input parameters. The adopted thickness of the flow near its source depends on an estimation of the topography beneath it, which can only be found by extrapolating the topographic contours around this part of the flow. That same extrapolation determines the mean slope down which the flow is moving, and so the slope and thickness estimates are directly proportionality to one another. Table 4 shows the result of adopting a plausible range of approximations to the topography underlying the proximal 50 m of the flow, before the flow ponds on the shallower floor of the Ina depression. Note that, because of the proportionality between the flow thickness and slope, the values of $W_b$ and $W_c$ do not change. The implied yield strengths vary by a factor of ~2 and the implied effusion rates and mound emplacement durations by a factor of ~3.5.

*5.4. Foam stage summary*

The treatments in Sections 5.2 and 5.3 have both assumed a Bingham rheology for the foam, but are based on completely different morphological measurements and assumptions, so it is relevant to compare them. Fig. 7 shows the relationship between foam effusion rate, $E$, and foam yield strength, $\tau_y$, from both treatments on the same graph. They intersect at ($\tau_y$ = 81.2 Pa, $E$ = 0.57 m$^3$ s$^{-1}$). If we take these values to represent the optimum solution, then interpolating from Tables 3 and 4 we find a foam bubble radius of $\varphi$ = 250.5 μm, a plate sinking speed of $U_P$ = 12.6 μm s$^{-1}$, and a mound formation time of $t_e$ = 12.6 days.

The travel time of any given batch of foam magma through the ~10 m thick crust at a speed of 11.15 mm s$^{-1}$ would have been ~15 minutes. For about half of this time the foam would have

ACCEPTED MANUSCRIPT


been in contact with the coolest, upper part of the crust and would have been losing heat to it at a rate controlled by the thermal diffusivity of the foam. The structure of the foam would have reduced the thermal diffusivity somewhat from dense rock values; the measurements of Bagdassarov and Dingwell (1994) suggest ~$5 \times 10^{-7}$ $m^2$ $s^{-1}$. Using equation (13) this would imply that cooling would have penetrated to a distance ~0.024 m into the foam from each wall of the fracture, so that about 30% of the first foam to emerge would have undergone cooling. Later, heat from the foam passing though the crack would have reduced the temperature difference between foam and lake crust, reducing the subsequent foam cooling rate. Heat loss does not seem to be critical in controlling the foam rheology, supporting our assumption that the surface tension of the foam is the key factor.

The morphology of the mounds on the floor of Ina (Figs. 1a, 6) is a function of both the rheology and the effusion rate of the foam. The combination of the yield strength of the foam and the low acceleration due to gravity on the Moon defines the thickness of the extruded lava and hence the heights of the mounds. The high viscosity and low effusion rate of the foam limits the lateral and axial spreading and leads to the bleb-like shape and steep sides (Figs. 1a, 6). This unusual low effusion rate and enhanced viscosity of the extruding basaltic foams emphasizes their mound-like shape, much as low effusion rate, viscous silicic flows produce dome-like constructs on Earth. We conclude that the formation of the mounds on the floor of the Ina summit pit crater (Figs. 1, 6) can be very plausibly interpreted as extrusion of magmatic foam through the cracked lava pond crust (Figs. 4, 5).

**6. Application to fissure vents**

The above stages in the development of a lunar eruption (Fig. 2) apply equally to fissure eruptions (Fig. 8), where localization of activity to one location or a small number of discrete vents does not take place. The line-source geometry in this case makes the formation of a coherent lava lake around the vent much less likely during the hawaiian and strombolian stages of activity. The sequence of events is therefore expected to be as follows. The earliest phase of the eruption forms lava flows with fairly uniform meso-vesicularity (Fig. 9) by coalescence of hot pyroclasts from the steady, or slightly pulsating, high volume flux lava fountain. These flows have the potential to travel for great distances due to the high volume flux feeding them. Subsequent reduction in the erupted volume flux as the dike begins to relax leads to a transition

ACCEPTED MANUSCRIPT


to a strombolian phase (Fig. 8). Lava continues to flow away from the fissure but now at a slower speed and with a very heterogeneous fabric due to its intermittent emergence from the fissure vent (Fig. 9). This lava consists in part of highly vesicular foam, in part of less vesicular lava where shear due to flow has coalesced and then collapsed water vapor bubbles, and in part of cooled clots of magma that have been ejected by large bursting CO bubbles, cooled in flight, and fallen back into the flow, further disturbing the flow fabric (Fig. 9). This lava is likely to have a very rough irregular surface texture. Finally the rise rate of magma at depth becomes negligible and the remaining, slow effusion from the vent is entirely due to the narrowing of the relaxing dike. No further strombolian activity occurs and the lava leaving the vent consists entirely of slow-moving water-vapor foam, suffering minimal disruption due to shear (Fig. 8).

**7. Discussion and Conclusions**

On the basis of the analysis of the theoretical treatment of the generation, ascent and eruption of basaltic magmas on the Moon (Wilson and Head, 2016) and the application of these principles to the interpretation of volcanic landforms and deposits (Head and Wilson, 2016), we examined the nature of the waning stages of eruptions forming small lunar shield volcanoes (Head and Gifford, 1980), their summit pit craters, and features in similar settings (elongate collapse craters and features in the lunar maria; Fig. 1). We reached the following conclusions:

1) Waning-stage formation of magmatic foams: In the waning stages of dike emplacement in small shield volcanoes and related eruptive environments, following the hawaiian phase (Figs. 2a-2c) and most of the strombolian eruptive phase (Figs. 2d, 3), stable magmatic foams are predicted to form (Figs. 2e, 4) due to exsolution of $H_2O$ and progressive reduction of magma rise rates. Foams collect in the top tens to hundreds of meters of the dike and in the lava lake (Figs. 2f, 4), and can have up to 95 volume % void space.

2) Waning-stage formation of chilled lava lake crust: As magma ascent slows through the strombolian phase, a chilled crust develops on the top of the lava lake (Fig. 3). The crust is predicted to be of the order of several meters thick and very vesicular, both at the microvesicular foam scale and at the macro-porosity scale due to the presence of large voids produced by crust deformation and disruption during the strombolian phase (Fig. 3). Local disruption of the foam by large strombolian-phase gas bubbles creates additional macro-porosity void space. This crust is developed on top of the evolving and growing foam (Fig. 4).

ACCEPTED MANUSCRIPT


3) Waning-stage extrusion of magmatic foams: As the dike overpressure relaxes and the dike attempts to close (Fig. 2e), the magmatic foam is forced out of the dike and into the base of the lava lake, stressing the growing chilled crust (Fig. 4). Cooling stresses also develop during this period. Flexing and fracturing of the chilled crust permits the foam to extrude out on top of the chilled crust to form convex mounds of foam (Figs. 2f, 4, 5), with simultaneous subsidence of the crust forming the depressed inner part of the summit pit crater. Popping of vesicles in the upper part of the extruded layer results in a decimeter- to meter-thick layer of fragments with sizes of a few tens of microns on top of the extruded foam (Fig. 5).

4) The nature of the final pit crater floor: At the end of the eruption, the final pit crater floor consists of the subsided chilled crust of the lava lake overlying unextruded magmatic foam, and the individual magmatic foam mounds, extruded through the chilled crust (Figs. 4, 5). Both the chilled crust and the foam mounds have very unusual physical properties (Fig. 9) compared with typical lunar mare basalt lava flows on which regolith is developed (Figs. 3-5). In contrast to the solid mare basalt flows (Fig. 9a) sampled by the Apollo astronauts, the chilled crust (Fig. 9b) would be extremely heterogeneous, very vesicular in some places, less so in others, and contain large void spaces developed during the strombolian and further cooling stages; it would also overlie a very porous micro-vesicular foam layer (Fig. 4). The mounds would consist of foams with up to 95 volume % void space, overlain by a layer of popped bubble wall shards (Figs. 5, 9c).

5) The subsequent evolution of the final pit crater floor: Mounds: The physical properties of the chilled crust and foam mounds have important implications for their subsequent modification (Figs. 8, 9). In contrast to the regolith typically developed on top of normal mare basalts, regolith-forming impacts on the foam (Fig. 9) will tend to crush the substrate rather than excavating and ejecting it, and superposed craters will tend to be smaller and less distinct (Schultz et al., 2002; Housen and Holsapple, 2003). Ejecta will not be spread laterally efficiently, helping to preserve the sharp margins of the mounds over time.

6) The subsequent evolution of the final pit crater floor: Hummocky/blocky floor unit: Impacts on the surface of the chilled crust of the lava lake floor will tend to compress the macro and micro-vesicularity and the macro-porosity of the crust and underlying foam immediately below the impact crater and shatter the most vesicular parts of the foam (Wunnemann et al., 2006), resulting in both poor crater retention and the creation of abundant space for regolith

ACCEPTED MANUSCRIPT


infiltration and drainage (Fig. 9b), assisted by seismic sifting from each subsequent impact (Yasui et al., 2015; Qiao et al., 2016a). These factors are a potential explanation for the relative optical immaturity of the blocky and hummocky floor units in Ina and related IMPs (e.g., Schultz et al., 2006); the extreme porosity of the chilled floor crust (Fig. 9) causes fine material to sift into the abundant underlying pore space, continuously exposing fresh blocks and severely retarding the buildup of a mature regolith (Qiao et al., 2016a).

7) Formation age of the mounds and hummocky/blocky floor material: On the basis of this analysis, the formation of mounds and hummocky/blocky floor material is a natural consequence of the low magma rise rates and degassing history of late-stage lunar basaltic eruptions that occurred several billion years ago. This is in contrast to the interpretation of Schultz et al. (2006) and Braden et al. (2014), that place their formation (or activity associated with their fresh-appearing characteristics) in the last 100 million years.

8) The apparent young age of the Ina interior mounds and other Irregular Mare Patches (IMPs): Taken together, these unusual characteristics of the terminal eruptive stage mounds and floor unit help to explain both the young crater retention ages of the Ina mounds and similar features reported by Braden et al. (2014) (less than 100 million years), and the relatively immature nature of the blocky areas of the pit crater floor lower unit (Qiao et al., 2016a). Craters forming in the foam will be significantly smaller in diameter and deeper than those in normal extrusive basalts (Fig. 9) because the foam will behave as an aerogel, distributing the impact energy very differently from an impact into a coherent target, and this will shift the impact crater size-frequency distribution-derived ages to significantly younger ages (Qiao et al., 2016a). Ongoing micrometeorite bombardment will reduce the depths of these craters but will not greatly change their diameters. Also, craters formed in the hummock/blocky floor material will be difficult to recognize and thus this surface will also appear artificially younger.

9) Application to other Irregular Mare Patches: These basic principles of waning-stage eruption behavior apply to all eruptions on the Moon, but will have different manifestations depending on the eruption environment. For example, lavas extruded from linear graben characterized by pit craters (Fig. 1b) will experience the same phases of late stage eruptions and should be characterized by the same types of lava crusts and foam extrusions. In a similar manner, linear fissure eruptions (e.g., Head and Wilson, 2016; their Figs. 12a, 12b) will undergo the same process of terminal dike closure and extrusion of magmatic foam (Fig. 8), but in this

ACCEPTED MANUSCRIPT


case the foam will not be extruded into a summit or elongate pit crater. Instead, the final effusive products are predicted to be 1) a rough-surfaced layer of strombolian ejecta mixed with very vesicular lava, followed by 2) overlying extruded magmatic foam eruptive structures distributed around and downslope from the vent, and surrounding the rough-surfaced strombolian ejecta to form kipukas (Fig. 1c). On the basis of typical dike widths and dike lengths, and the cooling-limited flow length treatment outlined above, we would anticipate that an extruded foam layer averaging 5 meters thick would cover an area of the order of 5-10 $km^2$, well within the range of dimensions reported by Braden et al. (2014) for dozens of Irregular Mare Patches (IMPs). We interpret the IMPs that lie within the maria (e.g., Fig. 1c), but are not associated with summit pit craters such as Ina, to be related to waning-stage magmatic foam eruptions from fissure vents formed during the main phases of mare basalt eruption history.

**Acknowledgements:**

We gratefully acknowledge the inspiration displayed by Apollo 15 Commander David R. Scott, when he initiated an unplanned stop on the trip back to the Lunar Module during the Apollo 15 mission to Hadley-Apennine in order to sample a spectacular highly vesicular basalt that he observed perched on the lunar surface (Apollo 15 Sample 15016, known as the "Seat Belt Basalt"; https://curator.jsc.nasa.gov/lunar/lsc/15016.pdf). Discussions with Commander Scott subsequent to the return of 15016 provided the motivation to study the formation of very highly vesicular basaltic foams, and to undertake the analysis reported here. We also gratefully acknowledge the importance of discussions with Le Qiao and his detailed analyses of Ina, Sosigenes and related irregular mare patches. We acknowledge financial support from the NASA Lunar Reconnaissance Orbiter Lunar Orbiter Laser Altimeter (LOLA) experiment (NNX09AM54G and NNX11AK29G to JWH) and the NASA Solar System Exploration Research Virtual Institute (SSERVI) grant for Evolution and Environment of Exploration Destinations under cooperative Agreement No. NNA14AB01A at Brown University.

ACCEPTED MANUSCRIPT


**Notation**

| Symbol | Definition | Value | Units |
|---|---|---|---|
| $d$ | mean pyroclast diameter | | m |
| $f$ | wall friction factor | $10^{-2}$ | dimensionless |
| $f_g$ | gas volume fraction in foam | | volume fraction |
| $g$ | acceleration due to gravity | 1.62 | m $s^{-2}$ |
| $m_{H2O}$ | molecular mass of $H_2O$ | 18.015 | kg $kmol^{-1}$ |
| $m_{CO}$ | molecular masses of CO | 28.010 | kg $kmol^{-1}$ |
| $n_{H2Od}$ | water solubility in magma | | mass fraction |
| $n_{H2Ot}$ | total magma water content | | mass fraction |
| $n_{H2Oe}$ | exsolved amount of water | | mass fraction |
| $q$ | ratio of plug width $W_{plug}$ to gap width $G$ | | dimensionless |
| $r$ | radius of circular vent conduit | | m |
| $t_e$ | duration of mound-forming eruption | | s |
| $u_g$ | gas speed in explosion products | | m $s^{-1}$ |
| $u_m$ | magma rise speed | | m $s^{-1}$ |
| $v_g$ | specific volume fraction of gas | | volume fraction |
| $v_m$ | specific volume fraction of liquid | | volume fraction |
| $w$ | width of elongate fissure vent | | m |
| $A$ | aspect ratio of dike or fissure | | dimensionless |
| $C$ | thickness of cooled crustal layer on lava pond | | m |
| $D_b$ | thickness of lava flow levée at channel edge | | m |
| $D_c$ | center-line depth of lava flow central channel | | m |
| $D_f$ | vertical extent of foam | | m |
| $D_p$ | thickness of layer of pyroclasts on foam surface | | m |
| $E$ | volume effusion rate of foam lava | | $m^3$ $s^{-1}$ |
| $F$ | length of elongate fissure vent | | m |
| $G$ | width of typical gap between crustal plates | | m |
| $L$ | length of side of crustal plate, assumed square | | m |
| $N_a$ | Avogadro's number | $6.0225 \times 10^{26}$ | $kmol^{-1}$ |
| $P$ | pressure | | Pa |
| $P_c$ | critical pressure for gas bubble rupture | | Pa |
| $P_d$ | pressure at which gas and pyroclasts decouple | | Pa |
| $P_{frag}$ | magma fragmentation pressure | | Pa |
| $P_n$ | pressure at which gas bubbles nucleate | | Pa |
| $P'$ | pressure gradient driving magma flow in dike | | Pa $m^{-1}$ |

ACCEPTED MANUSCRIPT


| | | | |
|---|---|---|---|
| $Q$ | universal gas constant | 8.314 | kJ $kmol^{-1}$ $K^{-1}$ |
| $S$ | optically thin outer fire fountain shell thickness | | m |
| $R$ | maximum pyroclast range | | m |
| $T$ | magma temperature | 1500 | K |
| $U_F$ | rise speed of foam between crustal plates | | m $s^{-1}$ |
| $U_P$ | sinking speed of crustal plate | | m $s^{-1}$ |
| $V$ | dense rock equivalent erupted volume flux | | $m^3$ $s^{-1}$ |
| $W$ | width of lava flow | | m |
| $W_b$ | width of levée of lava flow | | m |
| $W_c$ | width of central channel of lava flow | | m |
| $W_{plug}$ | width of unsheared plug in rising foam | | m |
| $W_t$ | total width of lava flow channel plus levées | | m |
| $X$ | length of lava flow | | m |
| $Z$ | thickness of lava flow | | m |
| $\alpha$ | slope of ground beneath lava flow | | radian |
| $\eta$ | lunar basaltic magma viscosity | 0.5 | Pa s |
| $\eta_B$ | plastic viscosity of foam | 500 | Pa s |
| $\kappa$ | thermal diffusivity of lava | $10^{-6}$ | $m^2$ $s^{-1}$ |
| $\phi_{CO}$ | effective diameter of CO molecules | $3.4 \times 10^{-10}$ | m |
| $\phi_{H2O}$ | effective diameter of $H_2O$ molecules | $3.8 \times 10^{-10}$ | m |
| $\rho_c$ | density of crustal layer on pond | 1500 | kg $m^{-3}$ |
| $\rho_f$ | density of foam at surface | | kg $m^{-3}$ |
| $\rho_m$ | density of magmatic liquid | 3000 | kg $m^{-3}$ |
| $\sigma$ | surface tension of magma | 0.37 | J $m^{-2}$ |
| $\tau_y$ | yield strength of foam | | Pa |
| $\varphi$ | gas bubble radius | | m |

ACCEPTED MANUSCRIPT

ACCEPTED MANUSCRIPT



**Table 1**

Steady explosive eruption phase. For combinations of the pre-eruption magma CO and $H_2O$ contents, $n_{COt}$ and $n_{H2Ot}$ , respectively, values are given for the eruption speed, $u_g$, the maximum pyroclast range, $R$, the thickness of the outer shell of the fire fountain from which heat can be radiated, $S$, and the implied volume flux, $V$, to produce the Ina feature, an example of a summit pit crater on a lunar shield volcano. See text for explanation.

| $n_{COt}$ /ppm | $n_{H2Ot}$ /ppm | $u_g$ /(m $s^{-1}$) | $R$ /m | $S$ /m | $V$ /($m^3$ $s^{-1}$) |
|---|---|---|---|---|---|
| 2000 | 1000 | 125.62 | 9740 | 8240 | 848 |
| 2000 | 795 or less | 118.33 | 8643 | 7143 | 725 |
| 1500 | 1000 | 114.07 | 8033 | 6533 | 660 |
| 1500 | 750 | 104.56 | 6748 | 5248 | 532 |
| 1500 | 649 or less | 100.58 | 6244 | 4744 | 485 |
| 1000 | 1000 | 101.74 | 6390 | 4890 | 498 |
| 1000 | 750 | 91.46 | 5163 | 3663 | 390 |
| 1000 | 500 | 80.40 | 3991 | 2491 | 301 |
| 1000 | 489 or less | 79.89 | 3940 | 2440 | 298 |
| 500 | 1000 | 88.39 | 4822 | 3322 | 363 |
| 500 | 750 | 77.08 | 3667 | 2167 | 280 |
| 500 | 500 | 64.67 | 2581 | 1081 | 234 |
| 500 | 301 or less | 53.69 | 1779 | 279 | 357 |
| 250 | 1000 | 81.22 | 4073 | 2573 | 307 |
| 250 | 750 | 69.25 | 2960 | 1460 | 244 |
| 250 | 500 | 55.90 | 1929 | 429 | 284 |
| 250 | 390 | 49.40 | 1508 | small | - |
| 0 | 1000 | 73.66 | 3349 | 1849 | 262 |
| 0 | 750 | 60.90 | 2287 | 787 | 237 |
| 0 | 550 | 49.38 | 1505 | small | - |

ACCEPTED MANUSCRIPT


**Table 2**

Foam stabilization stage. Values of the water vapor pressure, $P_f$, in bubbles near the surface of a magmatic foam with 95% vesicularity as a function of the total pre-eruption magma water mass fraction, $n_{H2Ot}$. The mass fraction of water exsolved into the vapor bubbles is $n_{H2Oe}$, the typical bubble radius is φ, and the capillary pressure preventing rupture of the foam is $P_c$. When $P_f$ exceeds $P_c$, as in the case for $n_{H2Ot}$ = 1000 ppm, a thickness $D_p$ of accumulated pyroclastic debris is needed to stabilize the foam. $P_n$ is the nucleation pressure for the total water content $n_{H2Ot}$ and $D_f$ is the depth of the base of the foam layer.

| $n_{H2Ot}$ | $P_f$ | $n_{H2Oe}$ | φ | $P_c$ | $D_p$ | $P_n$ | $D_f$ |
|---|---|---|---|---|---|---|---|
| /ppm | /kPa | /ppm | /μm | /kPa | /m | /kPa | /m |
| 1000 | 88.0 | 803 | 21.7 | 68.2 | 6.3 | 899 | 685 |
| 500 | 41.9 | 383 | 16.8 | 88.0 | not needed | 334 | 285 |
| 250 | 19.8 | 181 | 18.4 | 80.4 | not needed | 124 | 121 |

ACCEPTED MANUSCRIPT

ACCEPTED MANUSCRIPT



**Table 3**

Foam effusion stage through cracks between crustal plates. For the range of possible values of $q$, the ratio of plug width to crack width for mafic lava foam treated as a Bingham material with plastic viscosity 500 Pa s, values are given for the plug width, $W_{plug}$: the foam yield strength, $\tau_y$; the typical gas bubble radius, $\varphi$; the rise speed of the unsheared plug, $U_{plug}$; the mean rise speed of the magma, $U_F$; the sinking speed of the plate, $U_F$; and the volume flux of magma feeding a mound forming on top of the crust, $E$.

| $q$ | $W_{plug}$ /m | $\tau_y$ /Pa | $\varphi$ /μm | $U_{plug}$ /(mm $s^{-1}$) | $U_F$ /(mm $s^{-1}$) | $U_P$ /(μm $s^{-1}$) | $E$ /($m^3$ $s^{-1}$) |
|---|---|---|---|---|---|---|---|
| 0.05 | 0.0085 | 9.8 | 2074 | 16.64 | 11.37 | 12.87 | 0.58 |
| 0.1 | 0.017 | 19.6 | 1037 | 16.51 | 11.56 | 13.08 | 0.59 |
| 0.2 | 0.034 | 39.2 | 519 | 16.01 | 11.74 | 13.29 | 0.60 |
| 0.3 | 0.051 | 58.9 | 346 | 15.18 | 11.64 | 13.17 | 0.59 |
| 0.4 | 0.068 | 78.5 | 259 | 14.01 | 11.21 | 12.69 | 0.57 |
| 0.5 | 0.085 | 98.1 | 207 | 12.51 | 10.42 | 11.80 | 0.53 |
| 0.6 | 0.102 | 117.7 | 173 | 10.67 | 9.25 | 10.47 | 0.47 |
| 0.7 | 0.119 | 137.4 | 148 | 8.51 | 7.66 | 8.67 | 0.39 |
| 0.8 | 0.136 | 157.0 | 130 | 6.00 | 5.60 | 6.34 | 0.29 |
| 0.9 | 0.153 | 176.6 | 115 | 3.17 | 3.06 | 3.47 | 0.16 |
| 0.95 | 0.1615 | 186.4 | 109 | 1.63 | 1.60 | 1.81 | 0.08 |

ACCEPTED MANUSCRIPT

ACCEPTED MANUSCRIPT



**Table 4**

Mound formation stage. For a range of estimates of the thickness, $D_c$, of the mound-forming foam lava extrusion and of the slope, sin $\alpha$, on which it was erupted, values are given for the corresponding foam yield strength, $\tau_y$; levee thickness, $D_b$; levee width, $W_b$; and central channel width, $W_c$. The corresponding product of volume effusion rate, $E$, and plastic viscosity, $\eta_B$, is converted to an explicit effusion rate by assuming a viscosity of 500 Pa s and used to find the eruption duration, $t_e$.

| sin $\alpha$ | $D_c$ /m | $\tau_y$ /Pa | $D_b$ /m | $W_b$ /m | $W_c$ /m | $(E\ \eta_B)$ /(Pa m$^3$) | $E$ /(m$^3$ s$^{-1}$) | $t_e$ /days |
|---|---|---|---|---|---|---|---|---|
| 0.055 | 5.5 | 64 | 4.8 | 43.5 | 28 | 178 | 0.36 | 20.2 |
| 0.060 | 6.0 | 76 | 5.2 | 43.5 | 28 | 252 | 0.50 | 14.3 |
| 0.065 | 6.5 | 89 | 5.7 | 43.5 | 28 | 347 | 0.69 | 10.4 |
| 0.070 | 7.0 | 104 | 6.1 | 43.5 | 28 | 466 | 0.93 | 7.7 |
| 0.075 | 7.5 | 119 | 6.5 | 43.5 | 28 | 614 | 1.23 | 5.8 |

ACCEPTED MANUSCRIPT


**References**

Bagdassarov, N., Dingwell, D., 1994. Thermal properties of vesicular rhyolite. Journal of Volcanology and Geothermal Research, 60, 179–191.

Blackburn, E. A., Wilson, L., Sparks, R. S. J., 1976. Mechanisms and dynamics of strombolian activity. Journal of the Geological Society of London, 132 (4), 429-440.

Braden, S. E., Stopar, J. D., Robinson, M. S., Lawrence, S. J., van der Bogert, C. H., Hiesinger, H., 2014. Evidence for basaltic volcanism on the Moon within the past 100 million years. Nature Geoscience, 7 (11), 787–791, doi:10.1038/NGEO2252

Dixon, J. E., 1997. Degassing of alkali basalts. American Mineralogist 82, 368–378.

Dollet, D., Raufaste, C., 2014. Rheology of aqueous foams. Comptes rendus de l'Académie des Sciences, Série IV, Physique, Astrophysique, 15 (8-9), 731–747.

Fagents, S. A., Wilson, L., 1996. Numerical modelling of ejecta dispersal from transient volcanic explosions on Mars. Icarus, 123 (2), 284–295.

Fielder, G., Guest, J. E., Wilson, L., Rogers, P. S., 1967. New data on simulated lunar material. Planetary and Space Science, 15 (11), 1653–1666.

Fogel, R., Rutherford, M., 1995. Magmatic volatiles in primitive lunar glasses, I, FTIR and EPMA analyses of Apollo 15 green and yellow glasses and revision of the volatile-assisted fire-fountain theory. Geochimica et Cosmochimica Acta, 59, 201–215.

Garry, W. B., Robinson, M. S., Zimbelman, J. R., Bleacher, J. E., Hawke, B. R., Crupler, L. S., Braden, S. E., Sato, H., 2012. The origin of Ina: evidence for inflated lava flows on the Moon. Journal of Geophysical Research, 117, E00H31, doi:10.1029/2011JE003981.

ACCEPTED MANUSCRIPT


Gaudin, D., Taddeucci, J., Scarlato, P., Moroni, M., Freda, C., Gaeta, M., Palladino, D. M., 2014. Pyroclast tracking velocimetry illuminates bomb ejection and explosion dynamics at Stromboli (Italy) and Yasur (Vanuatu) volcanoes. Journal of Geophysical Research Solid Earth, 119, 5384–5397, doi:10.1002/2014JB011096.

Hauri, E. H., Weinreich, T., Saal, A. E., Rutherford, M. C., Van Orman, J. A., 2011. High pre-eruptive water contents preserved in lunar melt inclusions. Science, 333, 213–215.

Hauri, E. H., Saal, A. E., Rutherford, M. C., Van Orman, J. A., 2015. Water in the Moon's interior: Truth and consequences. Earth and Planetary Science Letters, 409, 252–264.

Head, J. W., Gifford, A., 1980. Lunar mare domes: Classification and modes of origin. Moon and Planets, 22, 235–258.

Head, J.W., Wilson, L., 1992. Lunar mare volcanism: Stratigraphy, eruption conditions, and the evolution of secondary crusts. Geochimica et Cosmochimica Acta, 56, 2155-2175.

Head, J. W., Wilson, L., 2016. Generation, Ascent and Eruption of Magma on the Moon: New Insights Into Source Depths, Magma Supply, Intrusions and Effusive/Explosive Eruptions (Part 2: Predicted Emplacement Processes and Observations). Icarus, doi:10.1016/j.icarus.2016.05.031.

Housen, K. R., Holsapple, K. A., 2003. Impact cratering on porous asteroids. Icarus, 163, 102–119, doi:10.1016/S0019-1035(03)00024-1.

Hulme, G., 1974. The interpretation of lava flow morphology. Geophysical Journal of the Royal Astronomical Society, 39, 361–383.

Ishibashi, H., Sato, H., 2010. Bingham fluid behavior of plagioclase-bearing basaltic magma: reanalysis of laboratory viscosity. Journal of Mineralogical and Petrological Sciences, 105, 334–339.

ACCEPTED MANUSCRIPT


Mader, H. M., Zhang, Y., Phillips, J. C., Sparks, R. S. J., Sturtevant, B., Stolper, E., 1994. Experimental simulations of explosive degassing of magma. Nature, 372, 85–88.

Mangan, M. T., Cashman, K. V., 1996. The structure of basaltic scoria and reticulite and inferences for vesiculation, foam formation, and fragmentation in lava fountains. Journal of Volcanology and Geothermal Research, 73, 1–18.

Michon, G. P., 2015. http://www.numericana.com/answer/ellipse.htm#15ppm Accessed on 8 May 2015.

Nicholis, M. G., Rutherford, M. J., 2006. Vapor/melt partitioning behavior of S and Cl in a C-O gas mixture. Lunar and Planetary Science XXXVII, abstract #2061.

Nicholis, M. G., Rutherford, M. J., 2009. Graphite oxidation in the Apollo 17 orange glass magma: Implications for the generation of a lunar volcanic gas phase. Geochimica et Cosmochimica Acta, 73, 5905–5917.

Parfitt, E. A., Wilson, L., 1995. Explosive volcanic eruptions - IX: The transition between Hawaiian-style lava fountaining and Strombolian explosive activity. Geophysical Journal International, 121 (1), 226–232.

Pinkerton, H., Wilson, L., 1994. Factors controlling the lengths of channel-fed lava flows. Bulletin of Volcanology, 56 (2), 108–120.

Qiao, L., Head, J., Wilson, L., Xiao, L., Kreslavsky, M., Dufek, J., 2016a. Ina Pit Crater on the Moon: Extrusion of Waning-Stage Lava Lake Magmatic Foam Results in Extremely Young Crater Retention Ages, Geology, in press, doi:10.1130/G38594.1.

ACCEPTED MANUSCRIPT


Qiao, L., Head, J., Wilson, L., Xiao, L., Dufek, J., 2016b. Sosigenes lunar irregular mare patch (IMP): Morphology, topography, sub-resolution roughness and implications for origin, Lunar and Planetary Science XLVII, abstract #2002.

Ramanujan, S., 1914. Modular equations and approximations to π. Quarterly Journal of Pure and Applied Mathematics (Oxford), 45, 350–372.

Rutherford, M. J., Head, J. W., Saal, A. E., Wilson, L., Hauri, E., 2015. A revised model for the ascent and eruption of gas-saturated lunar picritic magma based on experiments and lunar sample data. Lunar and Planetary Science XLVI, abstract #1446.

Saal, A. E., Hauri, E. H., Lo Cascio, M., Van Orman, J. A., Rutherford, M. C., Cooper, R. F., 2008. Volatile content of lunar volcanic glasses and the presence of water in the Moon's interior. Nature, 454 (7201), 192–195.

Sato, M., 1976. Oxygen fugacity and other thermochemical parameters of Apollo 17 high-Ti basalts and their implications on the reduction mechanism. Proceedings of the Lunar Science Conference 7, 1323–1344.

Sato, M., 1979. The driving mechanism of lunar pyroclastic eruptions inferred from the oxygen fugacity behavior of Apollo 17 orange glass. Proceedings of the Lunar Science Conference 10, 311–325.

Savage, W. Z., 1978. The development of residual stress in cooling rock bodies. Geophysical Research Letters, 5 (8), 633–636.

Schultz, P.H., Anderson, J.L.B., Heineck, J.T., 2002. Impact crater size and evolution: expectations for Deep Impact. Lunar and Planetary Science Conference XXXIII, abstract number 1875.

ACCEPTED MANUSCRIPT


Schultz, P.H., Staid, M.I., and Pieters, C.M., 2006, Lunar activity from recent gas release: Nature, v. 444, p. 184-186, doi:10.1038/nature05303.

Self, S., Wilson, L., Nairn, I. A., 1979. Vulcanian eruption mechanisms. Nature, 277 (5696), 440–443.

Self, S., Sparks, R. S. J., Booth, B., Walker, G. P. L., 1974. The 11973 Heimaey strombolian scoria deposit, Iceland. Geological Magazine, 111, 539–548.

Skelland, A.H.P., 1967. Non-Newtonian Flow and Heat Transfer. John Wiley & Sons, New York, 469 pp.

Solomon, S. C., Head, J. W., 1980. Lunar mascon basins:lava filling, tectonics, and evolution of the lithosphere. Reviews of Geophysics and Space Physics, 18 (1), 107–141.

Sparks, R. S. J., 1978. The dynamics of bubble formation and growth in magmas. Journal of Volcanology and Geothermal Research, 3, 1–37.

Strain, P., and El-Baz, F., 1980, The geology and morphology of Ina, *in* Proceedings, 11th Lunar and Planetary Science Conference: Houston, Texas, Lunar and Planetary Institute, p. 2437–2446.

Taylor, G. J., Warren, P., Ryder, G., Delano, J., Pieters, C., Lofgren, G., 1991. Lunar Rocks, Ch. 6 in Lunar Source Book, eds. Grant H. Heiken, David T. Vaniman and Bevan M. French, Cambridge University Press.

Turcotte, D. L., Schubert, G., 2002. Geodynamics. Cambridge University Press, 456 pp.

Viana, F., Pardo, R., Yánez, R., Trallero, J. L., Joseph, D. D., 2003. Universal correlation for the rise velocity of long gas bubbles in round pipes. Journal of Fluid Mechanics, 494, 379–398.

ACCEPTED MANUSCRIPT


Wetzel, D.T., Hauri, E. H., Saal, A. E., Rutherford, M. C., 2015. Carbon content and degassing history of the lunar volcanic glasses. Nature Geoscience, 8, 755–758, doi:10.1038/ngeo2511

Wieczorek, M. A., Neumann, G. A., Nimmo, F., Kiefer, W. S., Taylor, G. J., Melosh, H. J., Phillips, R. J., Solomon, S. C., Andrews-Hanna, J. C., Asmar, S. W., Konopliv, A. S., Lemoine, F. G., Smith, D. E., Watkins, M. M., Williams, J. G., Zuber, M. T., 2013. The crust of the Moon as seen by GRAIL. Science, 339, 671–675. doi: 10.1126/science.1231530 .

Wilson, L., Head, J.W., 1981. Ascent and eruption of basaltic magma on the Earth and Moon. Journal of Geophysical Research, 86 (B4), 2971–3001.

Wilson, L., Head, J.W., 1983. A comparison of volcanic eruption processes on Earth, Moon, Mars, Io and Venus. Nature, 302 (5910), 663-669.

Wilson, L., Head, J. W., 2001. Lava fountains from the 1999 Tvashtar Catena fissure eruption on Io: Implications for dike emplacement mechanisms, eruption rates and crustal structure. Journal of Geophysical Research, 106 (E12), 32997–33004.

Wilson, L., Head, J. W., 2016. Generation, ascent and eruption of magma on the Moon: New insights into source depths, magma supply, intrusions and effusive/explosive eruptions (Part 1: Theory). Icarus, http://dx.doi.org/10.1016/j.icarus.2015.12.039.

Wilson, L., Keil, K., 1997. The fate of pyroclasts produced in explosive eruptions on the Asteroid 4 Vesta. Meteoritics and Planetary Science, 32, 813–823.

Wilson, L., Keil, K., 2012. Volcanic activity on differentiated asteroids: A review and analysis. Chemie der Erde (Geochemistry), 72 (4), 289–322. doi:10.1016/j.chemer.2012.09.002

ACCEPTED MANUSCRIPT


Wilson, L., Mouginis-Mark, P. J., 2014. Dynamics of a fluid flow on Mars: Lava or mud? Icarus, 233, 268–280.

Wünnemann, K., Colins, G. S., Melosh, H. J., 2006. A strain-based porosity model for use in hydrocode simulations of impacts and implications for transient crater growth in porous targets. Icarus, 180 (2), 514-527.

Yasui, M., Matsumoto, E., Arakawa, M, 2015. Experimental study on impact-induced seismic wave propagation though granular materials. Icarus, 260, 320-331.

ACCEPTED MANUSCRIPT

ACCEPTED MANUSCRIPT


**Figure captions:**

**Fig. 1.** The nature and characteristics of several "irregular mare patches" (Braden et al., 2014). (a) Ina (18.65° N, 5.30° E), a 2-3 km pit crater atop an ~23 km diameter small shield volcano (Garry et al., 2012; Qiao et al., 2016a) (LROC NAC M119815703). (b) Sosigenes (8.34° N, 19.07° E), an elongate pit crater 7 × 3 km in dimensions (Qiao et al. 2016b) (LROC NAC M1114042961). (c) A small irregular mare patch in western Mare Tranquillitatis (9.58° N, 25.51° E; number 13 in Braden et al., 2014) (LROC NAC M1096329585).

**Fig. 2.** The successive stages of a lunar shield-building eruption (Gifford and Head, 1980) (a-c) and the critical final stages as the volume flux declines, and the summit pit experiences a strombolian eruptive phase and formation and emplacement of magmatic foam mounds (d-f) (Head and Wilson, 2016). Not to scale.

**Fig 3.** Processes operating in the late stages of the formation of a lunar shield volcano. The strombolian stage of lava lake evolution (left text) and development of the lava lake crust (right text), showing details of the stage illustrated in Fig. 2d.

**Fig. 4**. Processes operating in the final stages of dike closure in a lunar shield volcano. Shown are foam accumulation in the upper part of the dike and lava lake, breaching of the chilled crust and the extrusion of a basaltic foam to form floor mounds are, illustrating details of the stage shown in Fig. 2e, f.

**Fig. 5.** Formation of foam mounds in late-stage lava lakes, showing details of processes in Fig. 4.

**Fig. 6.** Image (a) and topographic profile (b) of a dome in northeast part of the Ina pit crater on the Moon ((see Fig. 1a). (a) is a portion of LROC NAC frame M119815703. Profile in (b) is from NAC DTM topography.

**Fig. 7.** The relationship between foam effusion rate, $E$, and foam yield strength, $\tau_y$, from the two treatments described in the text. The curves intersect at ($\tau_y$ = 81.2 Pa, $E$ = 0.57 $m^3$ $s^{-1}$).

**Fig. 8.** Sequence of events and stratigraphy for a fissure eruption**.** Note the similar stages to

ACCEPTED MANUSCRIPT


those illustrated for a pit crater on a small shield volcano (Fig. 1), but due to the lack of a confining summit pit crater, the magmatic foam extrudes as a broader, flow-like deposit**.** Flow of the final-stage magmatic foam over the late strombolian stage blocky and macro-porous and macro-vesicular lavas, forming kipukas between the foam mounds/lobes, helps to explain the nature of many of the IMP deposits reported in the lunar maria by Braden et al. (2014) (e.g., Fig. 1c).

**Fig. 9.** Substrate characteristics (top) of (a) normal basaltic lava flows, (b) lava lake crusts and (c) extruded foam mounds. Bottom of each diagram (a-c) shows the nature and characteristics of subsequent impact craters formed on their surfaces. The fundamental differences in the physical properties of these substrates, and their response to subsequent impacts, helps to explain the relative optical immaturity and the very low crater retention ages reported for the irregular mare patches (IMPs) (Schultz et al., 2006; Braden et al., 2014). In this scenario, the mounds and hummocky/blocky terrain form at the same time as the related mare features over 3 billion years ago, but the unusual substrate characteristics produce an artificially young crater retention age (<100 million years; Braden et al., 2014) and helps inhibit optical maturation.

ACCEPTED MANUSCRIPT

ACCEPTED MANUSCRIPT



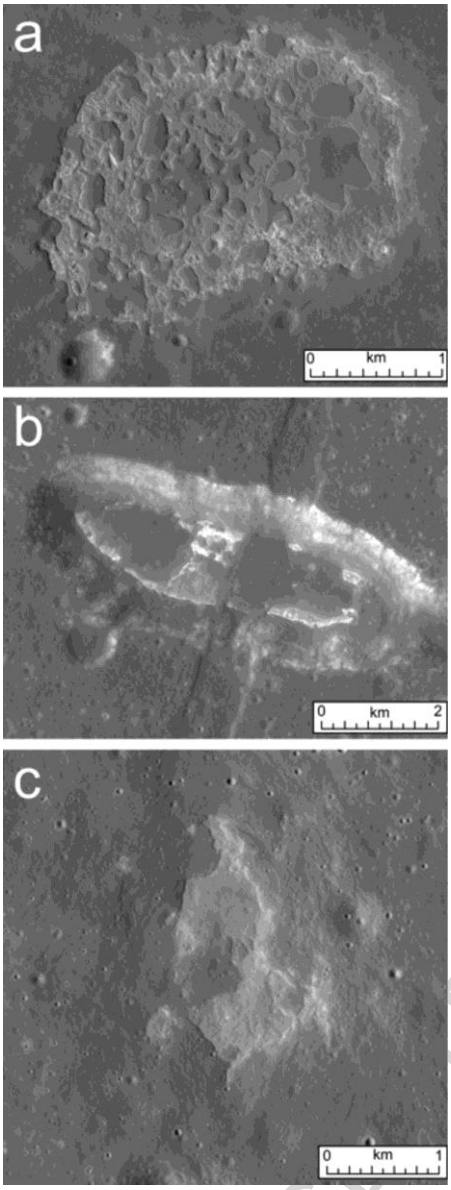


Fig. 1

ACCEPTED MANUSCRIPT

ACCEPTED MANUSCRIPT



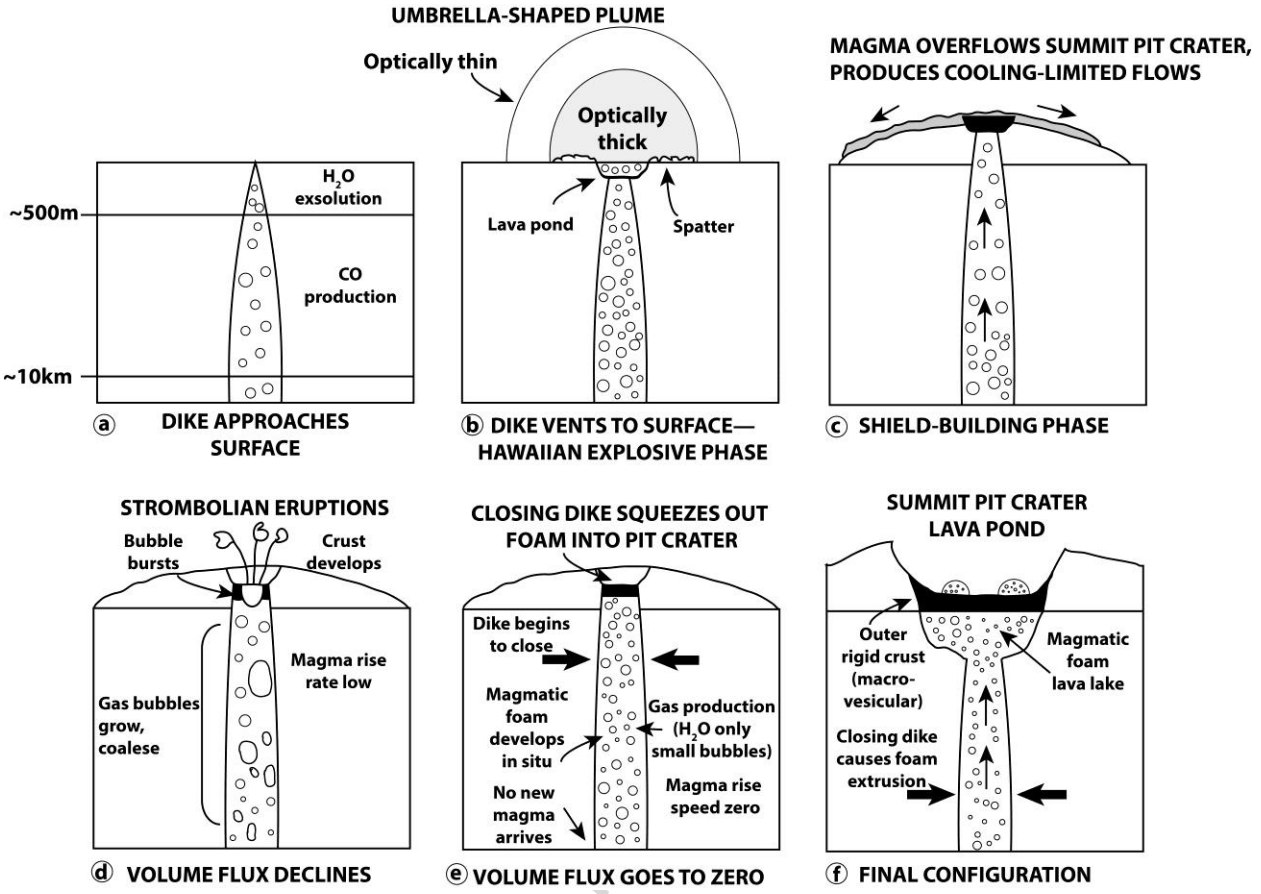


Fig. 2

ACCEPTED

ACCEPTED MANUSCRIPT



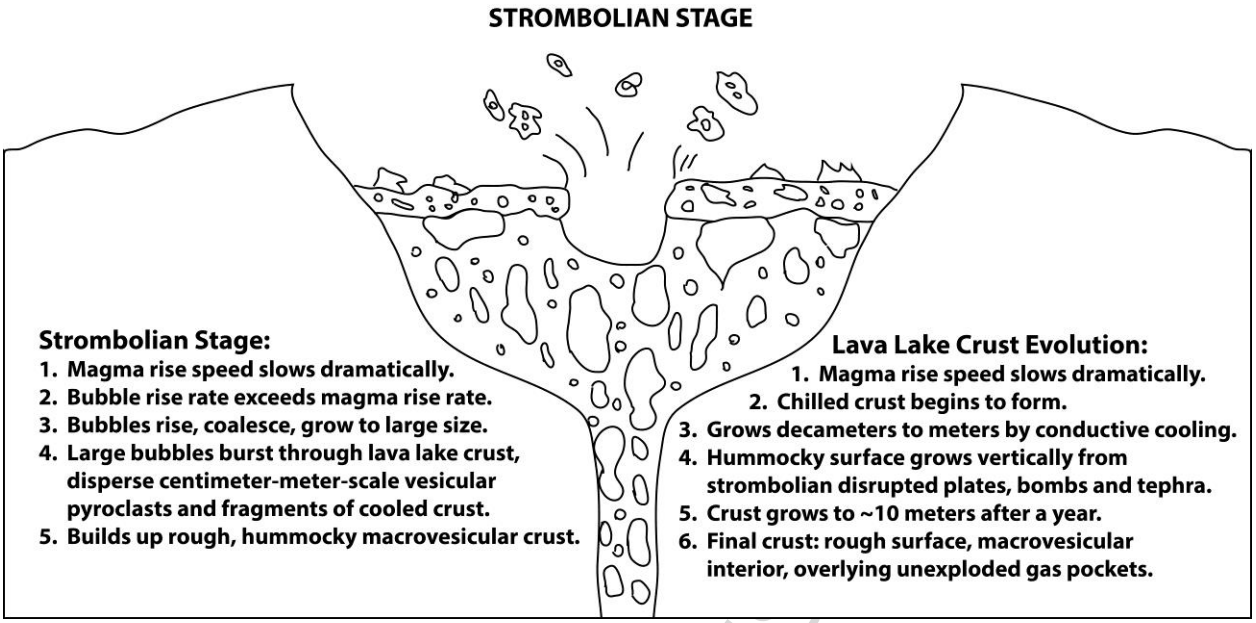


Fig. 3

ACCEPTED MANUSCRIPT

ACCEPTED MANUSCRIPT



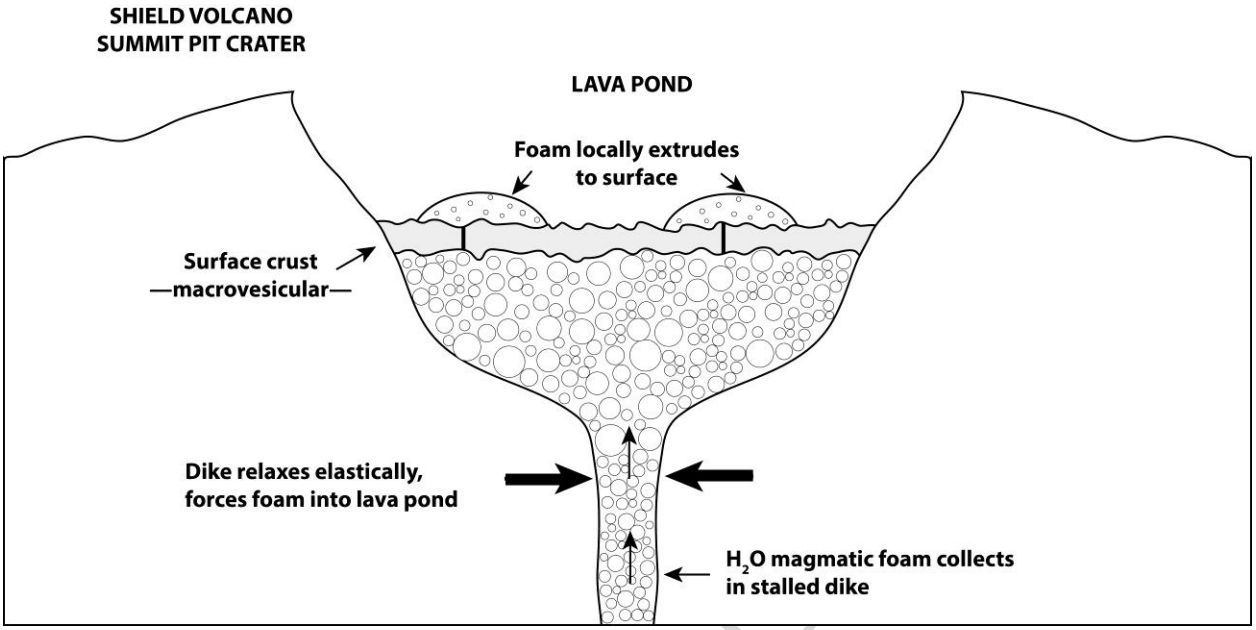


Fig. 4

ACCEPTED MANUSCRIPT

ACCEPTED MANUSCRIPT



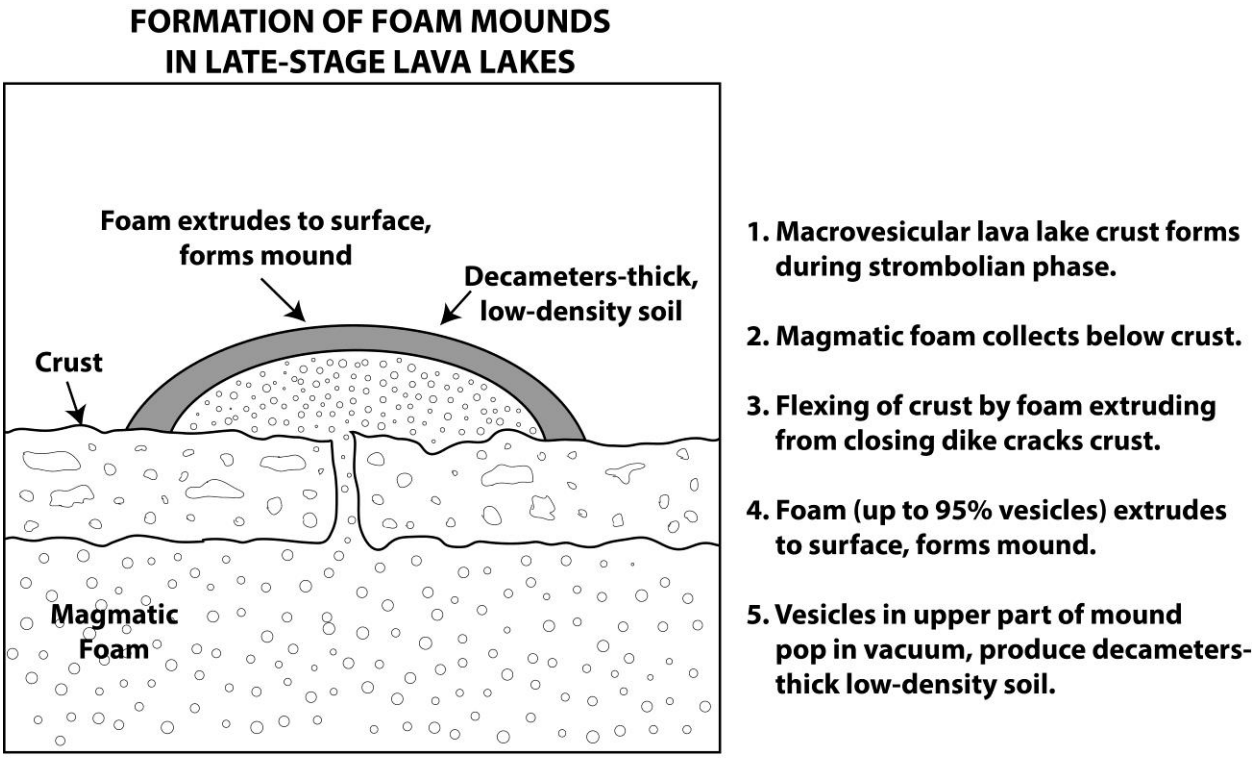


Fig. 5

ACCEPTED M

ACCEPTED MANUSCRIPT



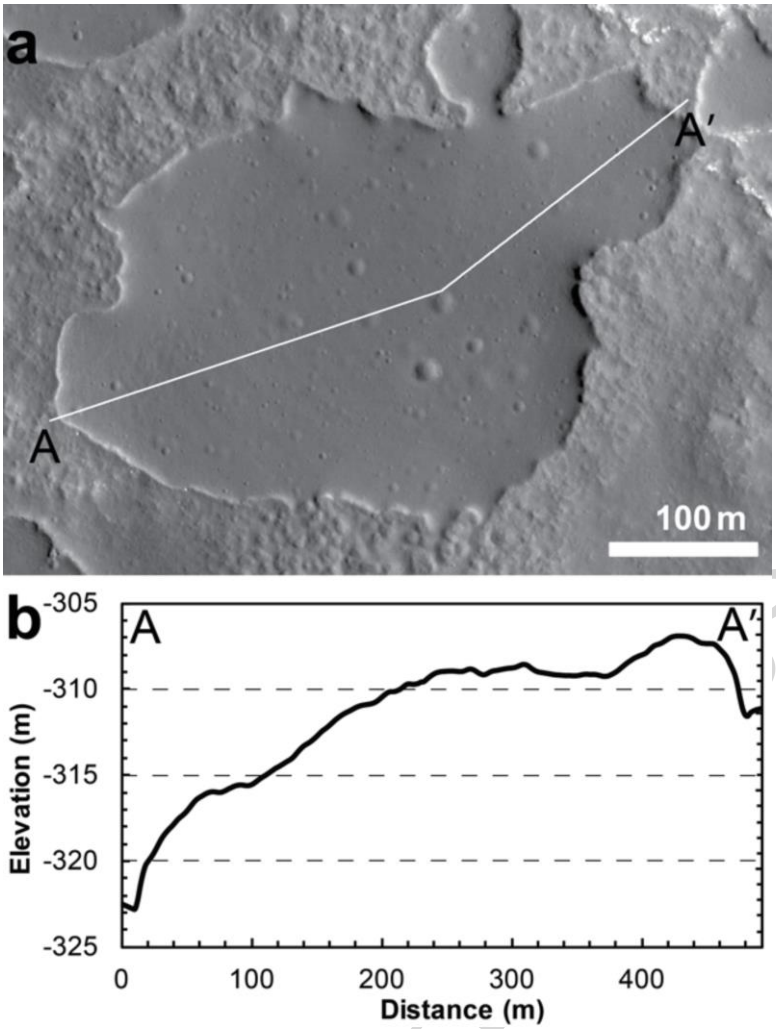


Fig. 6

ACCEPTED MANUSCRIPT

ACCEPTED MANUSCRIPT



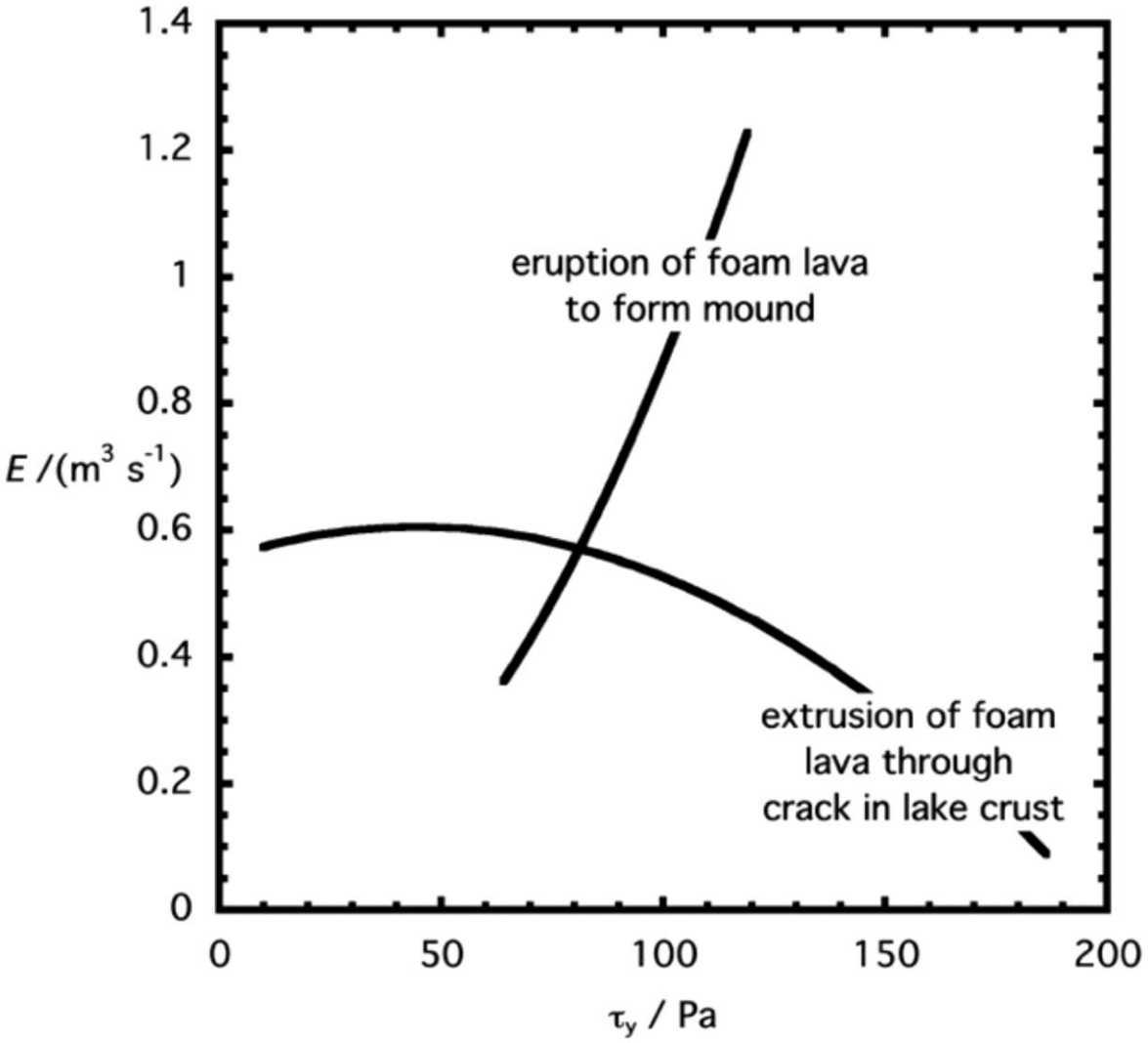


Fig. 7

ACCE

ACCEPTED MANUSCRIPT



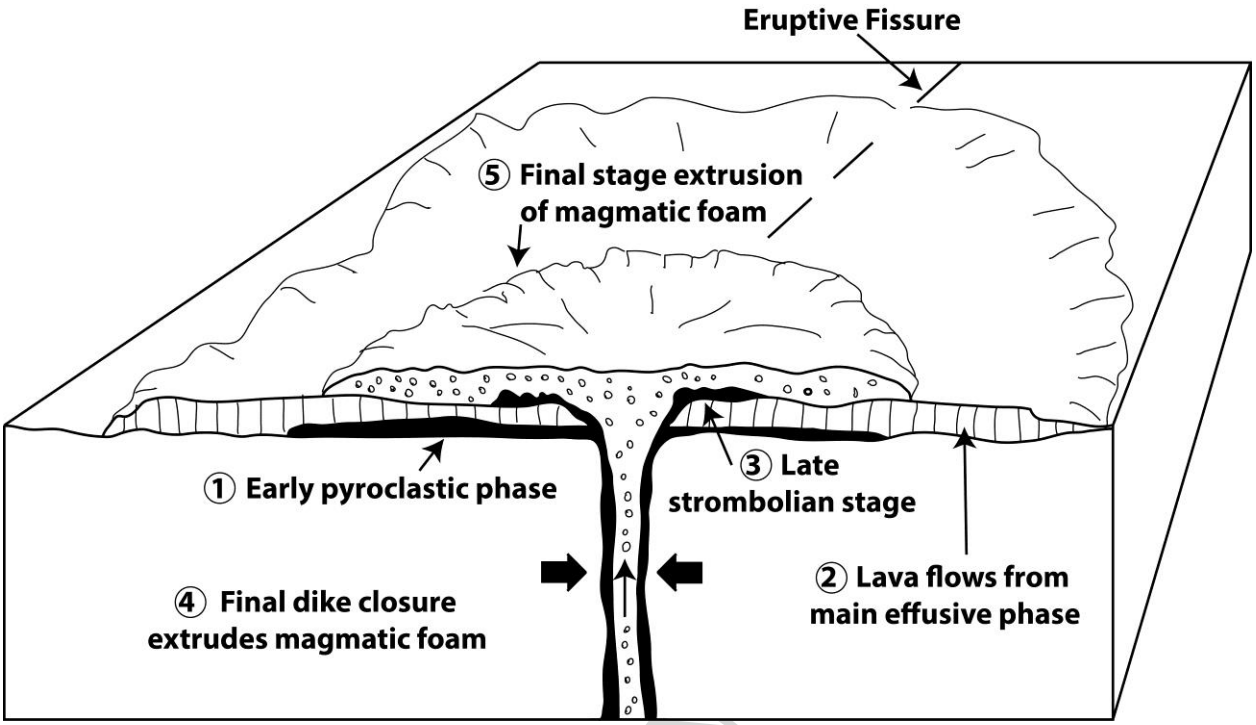


Fig. 8

ACCEPTED MANUSCRIPT

ACCEPTED MANUSCRIPT



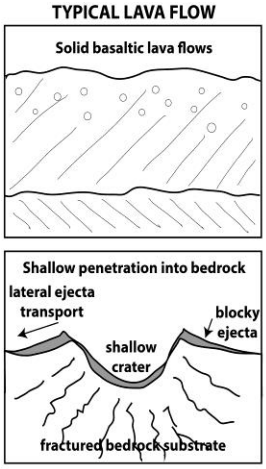


(a) Typical Lava Flow:
Top: Emplacement Phase:
1. Lava flow emplaced during main eruptive phase.
2. Pyroclasts coalesce to form flow, lava flows laterally, chills, solidifies.
3. Produces low porosity, low vesicularity, solid substrate.

Bottom: Regolith-Building Phase:
1. Subsequent impacts form in solid bedrock substrate.
2. Energy partitioning focused on fracturing, brittle deformation, comminution, ejection of solid particles.
3. Produces well-formed, relatively shallow, blocky craters, lateral ejecta.
4. Crater preservation favored.
5. Result: Typical mare regolith, fragmental ejecta layer buildup, optical maturity from accumulation of impact-melt-welded agglutinates, micrometeorite degradation of boulders.

(b) Pit Crater Floor:
Top: Emplacement Phase:
1. Pit crater floor is lava lake cooling thermal boundary layer, modified by impact of strombolian ejecta.
2. Solidifies, grows to meters-thick layer in less than a year.
3. Top of crust consists of rough surface of solid and macro/micro-vesicular blocks ejected by strombolian bubble bursts; macro-porosity among, between blocks.
4. Bottom of crust consists of cooling and downward-growing layer of macro-vesicles from larger coalesced vapor bubbles and meso-vesicles from smaller bubbles.
5. Chilled lava lake crust then overlies trapped bubbles and magmatic foam.

Bottom: Regolith-Building Phase:
1. Subsequent impacts form In macro-porous, macro/meso-vesicular substrate.
2. Energy partitioning focused on crushing of substrate that is extremely porous at a variety of scales, breakdown of bubble walls, excavation of blocky parts of strombolian substrate; lateral ejection is inhibited.
3. Craters in porous/vesicular portions produce hummocky substrate; those in coarser substrate produce blockier ejecta.
4. Extremely porous nature of the substrate at several different scales results in sifting of finer regolith particles (broken bubble walls, comminuted vesicular debris) into substrate; this retards surface regolith buildup and regolith optical maturation.
5. Subsequent impacts induce further "seismic sifting" of fines into substrate, maintaining "fresh" appearance of hummocky/blocky terrain.
6. Result: Craters are poorly formed, difficult to recognize, and degrade rapidly; seismic sifting into extremely porous substrate enhances loss of fines, exposes blocks, and obscures craters.

(c) Foam Mounds:
Top: Emplacement Phase:
1. Viscous magmatic foam (micro-vesicular) extruded through cracks in lava lake floor at low effusion rates as dike relaxes and closes.
2. Viscous foams extrude vertically, flow and spread laterally, coalesce, to produce mounds.
3. Mounds may initially be covered with decimeters thick layer of popped vesicles.
4. Lava lake crust may flex, subside below erupted foam mounds due to loading.

Bottom: Regolith-Building Phase:
1. Subsequent impacts form in solidified magmatic foam.
2. Energy partitioning favors foam penetration (the aerogel effect) and foam crushing over brittle deformation, crater formation and lateral ejection.
3. Regolith formation is dominated by poorly formed and anomalously small diameter superposed craters, and minimal lateral transport of any ejecta.
4. Result: Regolith dominantly non-blocky, formed of crushed and broken micro-vesicles, craters are much smaller, poorly preserved, easily degraded; little lateral ejection (aided by seismic sifting in adjacent hummocky/blocky terrain) retains sharp mound boundaries. The combination of processes yields anomalously young crater retention ages even though mounds formed at the same time as adjacent pit crater floor and shield volcano.

Fig. 9

ACCEPTED MANUSCRIPT


Highlights
VOLGEO_2016_134
Wilson and Head

1. Ina is an Irregular mare patch (IMP) with fresh-appearing mounds/hummocky material.

2. IMPs are interpreted to be young (<100 Ma), but Ina is atop a 3.5 Ga shield volcano.

3. Waning eruptive rise rates slow, more volatiles exsolve, as the dike begins to close.

4. This forms a very vesicular foam that can extrude to produce the mounds.

5. Unusual foam cratering properties (aerogel effect) can explain apparent young age.

ACCEPTED MANUSCRIPT